

Role of oceanic ozone deposition in explaining short-term variability of Arctic surface ozone at high-Arctic sites

Johannes G.M. Barten¹, Laurens N. Ganzeveld¹, Gert-Jan Steeneveld¹, and Maarten C. Krol^{1,2}

¹Wageningen University, Meteorology and Air Quality Section, Wageningen, the Netherlands

²Institute for Marine and Atmospheric Research Utrecht, Utrecht University, Utrecht, the Netherlands

Correspondence: Johannes G.M. Barten (sjoerd.barten@wur.nl)

Abstract. Dry deposition is an important removal mechanism for tropospheric ozone (O_3). Currently, O_3 deposition to oceans in atmospheric chemistry and transport models (ACTMs) is generally represented using constant surface uptake resistances. This is despite the fact that considering the role of solubility, waterside turbulence and O_3 reacting with ocean water reactants such as iodide ~~and dissolved organic matter~~ results in substantial spatiotemporal variability in O_3 deposition and concentrations in marine boundary layers. We hypothesize that O_3 deposition to the ~~cold~~ Arctic ocean, ~~with having a~~ relatively low reactivity, is ~~also~~ overestimated in current models with consequences for ~~background tropospheric~~ concentrations, lifetime ~~of~~ O_3 and long-range transport of O_3 . In this study, we investigate the ~~role impact~~ of the representation of oceanic O_3 deposition to the simulated magnitude and spatiotemporal variability in Arctic surface O_3 . ~~This study also serves as a preparatory study to understand the year-round Arctic O_3 concentration and deposition flux measurements as part of the MOSAiC field campaign. Furthermore, it is also important to enhance our understanding and quantification of Arctic ocean-atmosphere exchange of O_3 and other climate-active trace gases given the anticipated opening of the Arctic ocean.~~

We have ~~coupled integrated~~ the Coupled Ocean-Atmosphere Response Experiment Gas transfer algorithm (COAREG) ~~to into~~ the mesoscale meteorology and atmospheric chemistry model Polar-WRF-Chem (WRF) ~~and introduced~~ which introduces a dependence of O_3 deposition on ~~ocean waterside turbulent mixing conditions and biogeochemical composition~~ ~~physical and biogeochemical drivers of oceanic O_3 deposition~~. We have also reduced the O_3 deposition to sea ice and snow. Here, we evaluate the performance of WRF and the CAMS reanalysis data against hourly-averaged surface O_3 observations at 25 sites (latitudes $> 60^\circ N$) including the ~~ASCOS Arctic Summer Cloud Ocean Study (ASCOS)~~ campaign observations. This is the first time such a coupled modelling system has been evaluated against hourly observations at Pan-Arctic sites to study the sensitivity of the deposition scheme to the magnitude and short-term temporal variability in Arctic surface O_3 . We also analyze the impact of nudging WRF to the synoptic conditions from the ECMWF ERA5 reanalysis data on simulated Arctic meteorology and comparison of observed and simulated O_3 concentrations.

We show that the more mechanistic representation of O_3 deposition over oceans and reduced snow/ice deposition improves simulated Arctic O_3 mixing ratios both in terms of magnitude but also regarding observed temporal variability. Using the newly implemented approach, O_3 deposition velocities have been simulated in the order of 0.01 cm s^{-1} compared to $\sim 0.05 \text{ cm s}^{-1}$ in the constant surface uptake resistance approach. The simulated ~~monthly-mean~~ spatial variability in the mechanistic approach (0.01 to 0.018 cm s^{-1}) expresses the sensitivity to chemical enhancement with dissolved iodide whereas the temporal variability

(up to $\pm 20\%$ around the mean) expresses mainly differences in waterside turbulent transport. The bias for all observational sites above 70°N reduced from -7.7 ppb to 0.3 ppb with nudging and the revision to ocean and snow/ice deposition. Our study confirms that O_3 deposition to high-latitude oceans and snow/ice is overestimated in current models generally overestimated in ACTMs. We recommend that a mechanistic representation of oceanic O_3 deposition is-should be used in ACTMs to improve the representation of Arctic surface O_3 concentrations in terms of magnitude and short-term temporal variability. The revised ocean-atmosphere exchange representation can be further refined using the MOSAiC flux measurements as well as complementary observations such as sea ice and ocean water iodide concentrations.

1 Introduction

Tropospheric Ozone (O_3) is the third most important greenhouse gas and a secondary air pollutant negatively affecting human health (Nuvolone et al., 2018) and plant growth (Ainsworth et al., 2012) and artificial materials such as rubber (Lee et al., 1996) due to its oxidative character. O_3 shows a large spatiotemporal variability due to its relatively short lifetime (3-4 weeks) in the free troposphere compared to other greenhouse gases. Its main sources are chemical production and entrainment from the stratosphere. Its main sinks are chemical destruction and deposition to the Earth's surface (Young et al., 2018; Tarasick et al., 2019). Understanding the Arctic O_3 budget is of particular interest because its remote location implies that anthropogenic sources and sinks are generally absent. This makes these background Arctic O_3 observations an excellent indicator for global trends (Helmig et al., 2007b; Gaudel et al., 2020) excellent indicators for global trend analysis (Helmig et al., 2007b; Gaudel et al., 2020; Cooper et al., 2014). In the Arctic, routine tropospheric O_3 observations indicate an increasing trend up to the early 2000s which is leveling off (Oltmans et al., 2013; Cooper et al., 2014) or decreasing at individual sites (Cooper et al., 2020) in the last decade (Oltmans et al., 2013; Cooper et al., 2014). This upward trend can be attributed to increased emissions of precursors in the mid-latitudes (Cooper et al., 2014) but also (Cooper et al., 2014; Lin et al., 2017), but also changes in O_3 deposition to vegetation as a result of droughts and heatwaves (Lin et al., 2020) and stratosphere-to-troposphere transport may have played a role (Pausata et al., 2012). Local emissions of precursors are expected to become an important source of Arctic O_3 concentrations due to the warming Arctic climate and increasing local economic activity (Marelle et al., 2016; Law et al., 2017). This stresses the need to better understand underlines the need for understanding the sources and sinks of Arctic tropospheric O_3 and to accurately represent them in atmospheric chemistry and transport models (ACTMs).

On the global scale, dry deposition accounts for $\sim 25\%$ of the total sink term (Lelieveld and Dentener, 2000) in ACTM simulations and is especially important for the O_3 budget in the Atmospheric Boundary Layer (ABL) because it occurs at the Earth's surface (Hardaere et al., 2015) (Kavassalis and Murphy, 2017; Lin et al., 2019, 2020). Dry deposition in such model assessments ACTMs is often represented as a resistance in series approach (Wesely, 1989). In this approach the total resistance r_t is the sum of three serial resistances: the aerodynamic resistance (r_a) representing turbulent transport to the surface, the quasi-laminar sub layer resistance (r_b) representing diffusion close to the surface and the surface resistance (r_s) expressing the efficiency of removal by the surface. The dry deposition velocity (V_d) is then evaluated as the reciprocal of r_t . The r_a term is independent of the chemical species and mainly depends on the stability of the atmosphere and friction velocity

60 (u_{*}) (Padro, 1996; Toyota et al., 2016). The r_b term also scales with u_{*} and varies with the diffusivity of the chemical species (Wesely and Hicks, 2000). For very soluble species or reactive species such as nitric acid uptake by the ocean water is very fast, expressed by a (i.e. r_s of ~ 0 s m⁻¹), implying that the other resistances determine r_t and thus V_d . Less soluble gases, like O₃, have a high r_s that mainly, in comparison to the relatively small $r_a + r_b$ term, that dominates the magnitude of the O₃ dry deposition velocity (V_{d,O_3}). Thus, accurately representing the surface uptake efficiency is of high importance of O₃ is crucial.

65 Even though Observed O₃ deposition to oceans (e.g. Chang et al., 2004; Clifford et al., 2008; Helmig et al., 2012) and coastal waters (e.g. Gallagher et al., 2001) is relatively slow compared to terrestrial surfaces, expressed by typically observed ocean V_{d,O_3} of (~ 0.01 - 0.1 cm s⁻¹ (e.g. Helmig et al., 2012)), especially compared to observed maximum V_{d,O_3} for forests up to 2 cm s⁻¹ (Fan et al., 1990). However, it plays a large role in the total O₃ deposition budget due to the large surface area of water bodies (Ganzeveld et al., 2009) (Ganzeveld et al., 2009; Hardacre et al., 2015). Recent experimental and modelling studies indicate the spatiotemporal variability in oceanic O₃ uptake efficiency (Ganzeveld et al., 2009; Helmig et al., 2012; Luhar et al., 2018). However, most models ACTMs often still use a constant O₃ surface uptake efficiency of 2000 cm s⁻¹ to water bodies, proposed by Wesely (1989), resulting in a simulated ocean V_{d,O_3} of ~ 0.05 cm s⁻¹. The observed V_{d,O_3} shows a larger variability including also a dependency on wind speed and Sea Surface Temperature (SST) (Helmig et al., 2012). The dependency on wind speed also expresses an enhancement of O₃ deposition due to waterside turbulence (Fairall et al., 2007).

70 75 This turbulence driven enhancement is complemented by a strong chemical enhancement of oceanic O₃ deposition associated with its chemical destruction through oxidation of ocean water reactants such as dissolved iodide and dissolved organic matter (DOM) (Chang et al., 2004). Mechanistic O₃ deposition representations in models include the physical and biogeochemical processes related to the exchange and destruction of O₃ in surface waters (Fairall et al., 2007, 2011; Ganzeveld et al., 2009; Luhar et al., 2017, 2018). Dissolved iodide is deemed to be the main reactant of O₃ in surface waters (Chang et al., 2004) and therefore often applied in these representations. Some studies only consider dissolved iodide as a reactant (Luhar et al., 2017; Pound et al., 2019) whereas Ganzeveld et al. (2009) also included DOM as one reactant contributing to the chemical enhancement of oceanic O₃ deposition. However, the role of DOM in oceanic O₃ deposition remains difficult to quantify and which appears to be mainly addressed by controlled laboratory measurements experiments or O₃ flux measurements at sites with elevated DOM water concentrations. Nevertheless, application of these more mechanistic ocean O₃ deposition representations illustrated the importance of a more explicit representation of O₃ dry deposition in ACTMs, not only regarding the impact on marine ABL O₃ concentrations and budget, but also to consider potentially important feedback mechanisms. For instance, the implementation of these mechanistic exchange methods in ACTMs indicates a $\sim 50\%$ reduction of the global mean V_{d,O_3} which affects the tropospheric O₃ burden (Pound et al., 2019). This mechanistic representation especially results in a simulated decrease in V_{d,O_3} to cold polar waters with relatively low reactivity. Simulated V_{d,O_3} can be as low as 0.01 cm s⁻¹ compared to the commonly applied V_{d,O_3} of 0.05 cm s⁻¹ in the constant surface uptake resistance approach (Pound et al., 2019). Regarding feedback mechanisms, consideration of the mechanisms that ultimately determine the efficiency of uptake and destruction of O₃ in ocean surface waters might also explain the release of halogen compounds into the ABL (Prados Roman et al., 2015). These halogen compounds halogens, in turn, are involved in O₃ depletion in the ABL and therefore reduce further uptake and destruction of O₃ in ocean surface waters implying existence of a negative feedback mechanism.

95 Up until now, earlier studies have mostly focused on the effects on the global scale (Ganzeveld et al., 2009; Luhar et al., 2017) using on global scale oceanic O_3 deposition (Ganzeveld et al., 2009; Luhar et al., 2017) mainly relied on the evaluation of monthly mean surface O_3 observations (Pound et al., 2019). However, the hypothesized reduction in O_3 deposition The implementation of these mechanistic exchange methods in ACTMs, in particular the method proposed by Luhar et al. (2018) using a two-layer model representation (compared to a bulk layer version by Ganzeveld et al. (2009)), results in a ~50% reduction of the global mean V_{d,O_3} which affects the tropospheric O_3 burden (Pound et al., 2019). The mechanistic representation in Pound et al. (2019) especially results in a simulated decrease in V_{d,O_3} to cold polar waters with relatively low reactivity. Simulated V_{d,O_3} can be as low as 0.01 cm s^{-1} compared to the commonly applied V_{d,O_3} of 0.05 cm s^{-1} in the constant surface uptake resistance approach (Pound et al., 2019). However, the hypothesized deposition reduction to cold waters is also expected to substantially affect Arctic ABL O_3 concentrations on shorter timescales and potentially improve operational Arctic

100 O_3 forecasts, e.g. the air quality forecasts by the Copernicus Atmosphere Monitoring Service (CAMS) (Inness et al., 2019). An improved representation of sub-monthly Arctic O_3 concentrations helps to constrain the background O_3 concentrations in terms of magnitude and variability whereas the

105 The evaluation of simulated oceanic O_3 deposition in the Arctic is hampered by a lack of O_3 ocean-atmosphere flux observations. Hence, evaluation of simulated O_3 deposition relies on evaluation of surface O_3 concentrations, not only regarding the simulated and observed magnitude but in particular on the highly resolved temporal variability. We hypothesize that on the daily and diurnal timescales these concentrations are largely controlled by temporal variability in the main physical drivers of oceanic O_3 deposition, e.g. atmospheric and waterside turbulence. Chemical enhancement of, e.g., iodide to O_3 deposition is anticipated to control more the long-term (weeks-months) baseline level of V_{d,O_3} associated with anticipated more long-term (e.g. seasonal) changes in ocean water biogeochemical conditions (Sherwen et al., 2019). This evaluation of Arctic 110 spatiotemporal O_3 concentrations in terms of magnitude and short- and long-term variability aims to better understand sinks, processes, feedbacks and impacts of Arctic air pollution (Arnold et al., 2016) and the role of long-range transport (e.g. Thomas et al., 2013; Marelle et al., 2018) versus local sources (e.g. Marelle et al., 2016; Law et al., 2017; Schmale et al., 2018). Furthermore, the anticipated projected opening of the Arctic ocean, as one of the key features of Arctic a result of climate change, urges to improve our understanding of Arctic ocean-atmosphere exchange. In this study we only focus This study focuses on 115 the ocean-atmosphere exchange of O_3 , but follow-up studies are planned with a focus on ocean-atmosphere exchange and ABL concentrations of other trace gases such as dimethylsulfide (DMS), which enhances cloud formation and is involved in many feedback mechanisms (Mahmood et al., 2019).

120 The main objective of this study is to address the role We aim to identify and quantify the impact of a mechanistic representation of O_3 deposition in explaining observed hourly Arctic surface O_3 concentrations, both in terms of magnitude and temporal variability. A mesoscale coupled meteorology-atmospheric chemistry model is set up for an end-of-summer period in 2008 and evaluated against a large dataset of pan-Arctic O_3 observations at a high resolution (hourly) timescale for the end-of-summer 125 2008. Having a much higher spatial and temporal resolutions compared to other global modelling studies we aim to better capture the role of spatiotemporal variability in O_3 deposition in explaining observed surface O_3 concentrations in particular particularly regarding temporal variability. We also indicate the role of meteorology in simulating these O_3 concentrations by

130 nudging the simulated synoptic conditions towards an atmospheric reanalysis dataset. ~~This study also serves as a preparatory study to understand the year-round Arctic O₃ concentration and deposition flux measurements including the role of the local meteorology such as boundary layer mixing and entrainment as part of the Multidisciplinary drifting Observatory for the Study of Arctic Climate (MOSAiC) campaign (, last access: 16 September 2020).~~ Section 2 describes the adjustments to the deposition scheme in the mesoscale ACTM, further model setup and observational datasets. Section 3 presents the main results of the
135 study which are further discussed in Sect. 4. This manuscript is finalized with the conclusions in Sect. 5.

2 Methods

2.1 Regional coupled meteorology-chemistry model

We use the Weather Research and Forecasting model (v4.1.1) coupled to chemistry (Chem) (Grell et al., 2005) and optimized for Polar regions (Hines and Bromwich, 2008). Polar-WRF-Chem (hereafter: WRF) is a non-hydrostatic mesoscale
140 numerical weather prediction and atmospheric chemistry model used for operational and research purposes. Figure 1 shows the selected study area including the locations of surface O₃ observational sites ~~that will be used in this study~~ selected for this study (more information in Sect. 2.3). WRF is set up with a polar projection centered at 90°N, 250×250 horizontal grid points (30×30 km resolution) and 44 vertical levels up to 100 hPa, with a finer vertical grid spacing in the ABL and lower troposphere. The simulation period is ~~08-08-2008 to 07-09-2008~~ 08-August-2008 to 07-September-2008 including three
145 days of spin-up. This end-of-summer 2008 period is chosen ~~for two reasons~~: 1) to limit the role of active halogen chemistry during springtime (Pratt et al., 2013; Thompson et al., 2017) (Pratt et al., 2013; Thompson et al., 2017; Yang et al., 2020) and 2) the additional availability of O₃ observations in the high Arctic over sea ice from the ASCOS campaign (Paatero et al., 2009). The ECMWF ERA5 meteorology (0.25°×0.25°) (Hersbach et al., 2020) and CAMS reanalysis chemistry (0.75°×0.75°) (In-
150 neness et al., 2019) products are used for the initial and boundary conditions. Boundary conditions, SSTs and sea ice fractions are updated every three hours to these reanalysis products to allow for the sea ice retreat during the simulation. Other relevant parameterization schemes and emission datasets have been listed in Tab. A1 and are mostly based on Bromwich et al. (2013).

2.1.1 Nudging to ECMWF ERA5

The first WRF simulation, without any adjustments to O₃ deposition, indicated that WRF was misrepresenting the temporal variability in surface O₃ observations, most prominently starting from a few days into the simulation. We hypothesize that ~~these deviations are this misrepresentation is~~ caused by deviations in the synoptic conditions in the free running WRF simulation.
155 ~~To verify this~~Hence, WRF results are compared against the observations from the Advanced Microwave Scanning Radiometer - Earth Observing System (AMSR-E) sensor on NASA's Aqua satellite. The near surface wind speeds above oceans from the Daily Level-3 data product are used with a spatial resolution of 0.25°×0.25° (Wentz and Meissner, 2004).
Figure 2 shows the temporal evolution in the bias (WRF minus AMSR-E) and Mean Absolute Error (MAE) of the daily and
160 ocean grid box averaged 10-m wind speeds. ~~The~~ Although the first days there is no clear bias. ~~However~~, later in the simulation

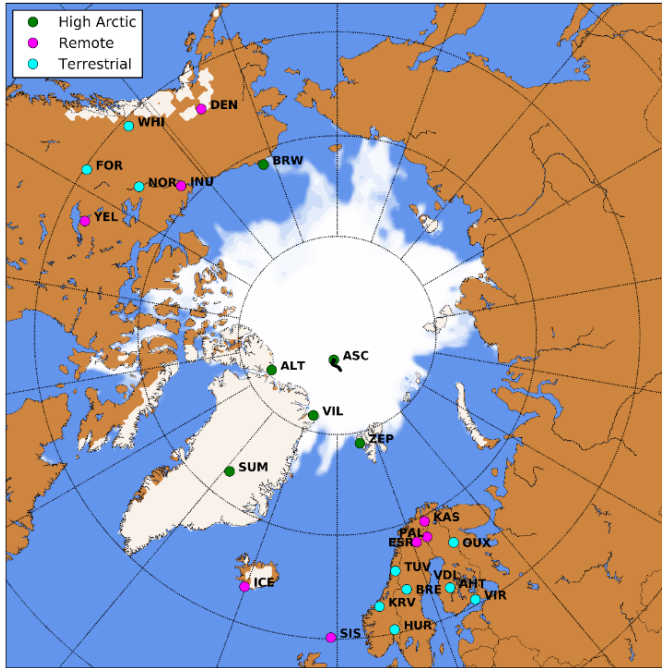


Figure 1. WRF domain including sea ice and snow cover at the start of the simulation. Locations with surface observations O_3 are indicated in green (High Arctic), magenta (Remote) and cyan (Terrestrial) (see Sect. 2.3). The drifting path of the ASCOS campaign during the simulation is indicated with the black line.

we find a persistent [positive wind speed](#) bias indicating that WRF overestimates the wind speeds above the Arctic ocean. During the first days the MAE amounts to $\sim 1.5 \text{ m s}^{-1}$, while later in the simulation the MAE reaches $2.5\text{--}3.0 \text{ m s}^{-1}$. To overcome the impact of this deficiency on our O_3 budget study, nudging is applied to ensure a fair model evaluation with observations. Hence, WRF is nudged every three hours to the ECMWF ERA5 humidity, temperature and wind fields in the free troposphere with nudging coefficients of $1\cdot 10^{-5} \text{ s}^{-1}$, $3\cdot 10^{-4} \text{ s}^{-1}$ and $3\cdot 10^{-4} \text{ s}^{-1}$, respectively. In Sect. 3.3 the [role-impact](#) of nudging on simulated surface O_3 is further analysed.

2.2 Representation of ocean-atmosphere gas exchange

The Coupled Ocean-Atmosphere Response Experiment (COARE) (Fairall et al., 1996) has been developed to study physical exchange processes (sensible heat, latent heat and momentum) at the ocean-atmosphere interface. Later, COARE has been extended to include the exchange of gaseous species such as O_3 , dimethyl sulfide (DMS) and carbon dioxide (CO_2) (Fairall et al., 2011). Many studies have used the COARE Gas transfer algorithm (COAREG) in combination with eddy covariance measurements to study the effects of wind speed and sea state on ocean-atmosphere gas exchange (e.g. Helmig et al. (2012), Blomquist et al. (2017), Bell et al. (2017), Porter et al. (2020)). Furthermore, the COAREG algorithm has also been previously used in global O_3 modelling studies Ganzeveld et al. (2009). The choice for COAREG as ocean-atmosphere exchange param-

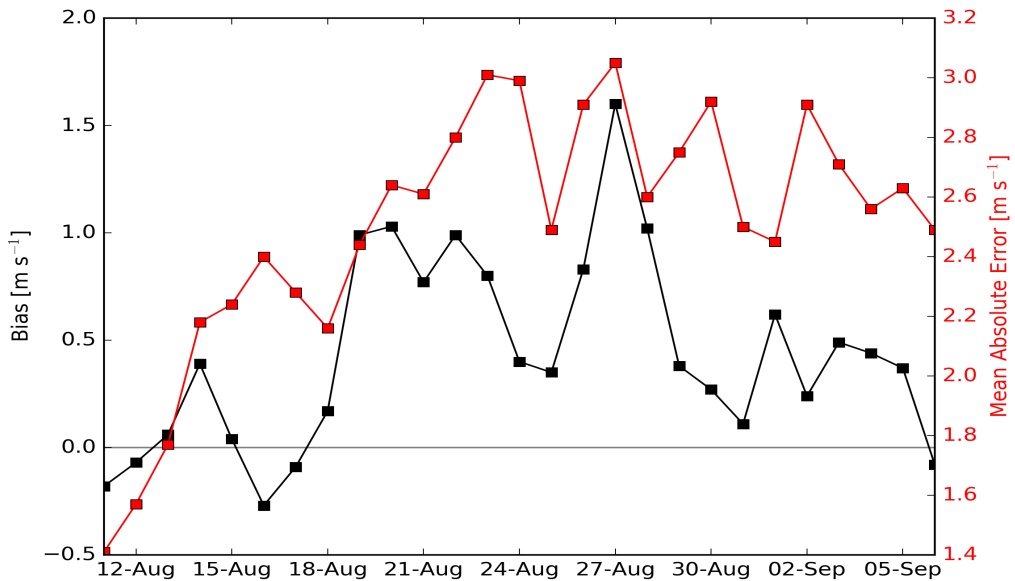


Figure 2. Temporal evolution of the bias (WRF minus AMSR-E, black) [m s^{-1}] and Mean Absolute Error (MAE, red) [m s^{-1}] of 10-m wind speeds above oceans for the period of 11-Aug to 6-Sep 2008. Note that the right y-axis starts at 1.4 m s^{-1} .

175 eterization is further motivated by the consistent coupling with other species such as DMS.

Here we use COAREG version 3.6, which is extended with a two-layer scheme for surface resistance compared to the previous version described by Fairall et al. (2007, 2011). ~~COAREG version 3.6 has already been used in a study by Porter et al. (2020) on air-sea transfer of highly soluble species.~~ The two-layer scheme is similar to ~~the work by~~ Luhar et al. (2018) building upon a first application of a 1-layer version of COAREG ~~for oceanic O_3 deposition in a global modelling study~~ by Ganzeveld et al.

180 In that study, chemical enhancement of ocean O_3 deposition by its reaction with iodide was considered using a global climatology of ocean surface water concentrations of nitrate serving as a proxy for oceanic iodide concentrations (I^-_{aq}), the compound that is generally deemed to be the most significant reactant for O_3 in ocean water (Chang et al., 2004). ~~Besides nitrate, satellite-derived chlorophyll- α concentrations have been used as a proxy for I^-_{aq} (Oh et al., 2008).~~ Since then, alternative parameterizations of oceanic I^-_{aq} have been proposed (e.g. MacDonald et al., 2014) using SST as a proxy for this reactant.

185 In COAREG, chemical reactivity of O_3 with I^-_{aq} is present through the depth of the oceanic mixing layer. O_3 loss by waterside turbulent transfer is negligible in the top water layer (few micrometers), but is accounted for in the underlying water column. The waterside turbulent transfer term is especially relevant for relatively cold waters because the chemical enhancement term is then relatively low (Fairall et al., 2007; Ganzeveld et al., 2009; Luhar et al., 2017). The last two important waterside processes that determine the total O_3 deposition are molecular diffusion and solubility of O_3 in seawater which both depend on the SST.

190 In Appendix B we list the formulation of the air- and waterside resistance terms in the COAREG routine applied in this study

and show the sensitivity to the environmental factors wind speed, SST and Γ_{aq} for typical Arctic conditions.

In this study, the COAREG algorithm is coupled such that WRF provides the meteorological and SST input for the COAREG routine. In turn, the COAREG calculated ocean-atmosphere exchange velocities are used in the WRF model to calculate the total flux. This study focuses on the exchange, in this case deposition, of O_3 . The oceanic O_3 deposition fluxes replace the default flux replacing the default oceanic O_3 deposition fluxes calculated by the Wesely (1989) scheme reflecting use of the default constant r_s of 2000 s m^{-1} . For grid boxes with fractional sea ice cover, COAREG replaces the Wesely deposition scheme for the fraction that is ice free. Note that in this study, only O_3 ocean-atmosphere exchange is represented by COAREG not having modified simulations of ocean-atmosphere exchange of other compounds (e.g. DMS).

Moreover, we apply the monthly-mean Γ_{aq} distribution by Sherwen et al. (2019) ($0.125^\circ \times 0.125^\circ$ resolution). This distribution does not only depend on SST, but which applies a machine learning approach, namely the Random Forest Regressor algorithm (Pedregosa et al., 2011), using various physical and chemical variables. For such as SST, nitrate and chlorophyll- α . This distribution replaces the previously applied Γ_{aq} estimations only using SST (Chance et al., 2014; MacDonald et al., 2014). At high latitudes, this implies higher these Γ_{aq} and thus higher distributions are highly uncertain due to the limited number of observations. However, the choice for Sherwen et al. (2019) is motivated by the most accurate representation of observed Γ_{aq} on the global scale. Figure C1 shows the spatial distribution of Γ_{aq} used in the calculation of the O_3 deposition compared to MacDonald et al. (2014). In that study velocities of COAREG coupled to the WRF model. Using the Sherwen et al. (2019) distribution for August/September we found relatively high Γ_{aq} concentrations ranging between 30 nM and 80 nM for the open oceans up to 130 nM in coastal waters. In MacDonald et al. (2014) and Chance et al. (2014), Γ_{aq} is solely a function of SST which leads to very small Γ_{aq} in the cold Arctic ocean order of 5 to 50 nM and thus low reactivity and O_3 deposition velocities. As mentioned previously, the study by Ganzeveld et al. (2009) also considered the potentially important enhancement in oceanic O_3 deposition by its reaction with DOM, a feature not considered in studies by Luhar et al. (2017); Pound et al. (2019). In Sect. 4 we will discuss the potential role of DOM in our simulations and Arctic O_3 deposition.

2.2.1 Deposition to snow and ice

Reported atmosphere-snow gas exchange spans a wide range of observed O_3 deposition velocities. Some studies even report episodes of negative deposition fluxes (emissions) over snow or sea ice (Zeller, 2000; Helmig et al., 2009; Muller et al., 2012). Clifton et al. (2020b) recently summarized observed O_3 deposition velocities to snow having a range of -3.6 to 1.8 cm s^{-1} with most of the observations indicating a deposition velocity between 0 and 0.1 cm s^{-1} for multiple snow covered surfaces (e.g. grass/forest/sea-ice). Generally, ozone concentrations in the interstitial air of the snowpack is lower than in the air above making it a not a direct source of O_3 in terms of emissions (Clifton et al., 2020b). However, the emissions of O_3 precursors from the snowpack can enhance O_3 production in the very stable atmosphere above the snowpack (Clifton et al., 2020b). Helmig et al. (2007a) investigated the sensitivity of a chemistry and tracer transport model to the prescribed O_3 deposition velocity and found best agreement between modelled and observed O_3 concentrations by applying deposition velocities in the order of 0.00 - 0.01 cm s^{-1} . Based on Following Helmig et al. (2007a) we have increased the O_3 surface uptake resistance (r_s) for snow and ice land use classes to 10^4 s m^{-1} . This corresponds to total deposition velocities of $\leq 0.01 \text{ cm s}^{-1}$, which is a reduction of

225 ~66% compared to the Wesely deposition routine that is the default being applied in WRF (Grell et al., 2005). Effects of this modification are further examined in Sect. 3.1.

2.3 Observational data of surface ozone

The new modelling setup, including nudging to ECMWF ERA5 and the revised O₃ deposition to snow, ice and oceans, is evaluated against observational data of pan-Arctic surface O₃ concentrations. We expect that the different representation of 230 O₃ deposition mostly affects O₃ concentrations in the ABL. Therefore, we evaluate our simulations against hourly averaged surface O₃ observations from 25 measurement sites above 60 °N. These sites are further categorized in three site selections: 'High Arctic', 'Terrestrial' and 'Remote'. High Arctic refers to sites having latitudes > 70 °N and for which we expect that the deposition footprint is a combination of ocean and (sea-)ice sea-ice (e.g. Helmig et al., 2007b). The Terrestrial sites are located below 70 °N and show a clear diurnal cycle in observed O₃ (e.g. Chen et al., 2018). These diurnal cycles are governed by 235 a combination of emissions of precursors, but also the anticipated larger diurnal cycle in O₃ deposition (Zhou et al., 2017) to, e.g., vegetated surfaces and a stronger diurnal cycle in turbulent mixing conditions and ABL dynamics. These are in all aspects different from sites that have an ocean/ice sea-ice footprint where we expect low emissions of precursors, no clear diurnal cycle in O₃ deposition and a weaker diurnal cycle in ABL dynamics (Van Dam et al., 2015). In this study, the criterion 240 is that the average observed minimum nighttime mixing ratio is > 8 ppb smaller than the average observed maximum daytime mixing ratio during the ~1 month of simulation. This criterion is based on a preparatory analysis of the observational data, footprint and site characteristics. The Remote sites are located have been identified as such based on their location below 70 °N and at which showing no clear diurnal cycle is observed in O₃ concentrations. The analysis also includes the observations 245 during the Arctic Summer Cloud Ocean Study (ASCOS) campaign, when the icebreaker Oden was located in the Arctic sea ice (Tjernstrom et al., 2012). In total, 25 surface O₃ measurement sites are included (Fig. 1) of which 6, 8 and 11 sites are characterized High Arctic, Remote and Terrestrial sites, respectively. A full list of available measurement sites is available in Tab. D1.

2.4 Overview of performed simulations

In total, we perform three simulations. The first WRF simulation (DEFAULT) is a run without any adjustments to the code as 250 described in Sect. 2.1. The second simulation (NUDGED) includes nudging of the synoptic conditions to the ECMWF ERA5 product as described in Sect. 2.1.1. The third simulation (COAREG) includes nudging, but also includes the adjustments to the O₃ deposition to oceans as described in Sect. 2.2 and the O₃ deposition to snow and ice as described in Sect. 2.2.1. Furthermore, we also compare our results with the the state-of-the-art CAMS global reanalysis data product (Inness et al., 2019). This product has a temporal resolution of 3 hours, a spatial resolution of 0.75°×0.75°, and does not include a mechanistic representation 255 of ocean-atmosphere O₃ exchange. Regarding O₃, CAMS assimilates satellite observations of O₃ but it does not assimilate O₃ observations from radiosondes or in situ measurement sites or radiosondes such as the 25 sites used in the here presented evaluation. Moreover, CAMS is being widely used for air quality forecasts and assessments but also to constrain regional scale modelling experiments such as presented in this study.

3 Results

First, we will present the spatial and temporal variation in O_3 dry deposition velocities (V_{d,O_3}) of the ~~new and default NUDGED~~ 260 and ~~COAREG~~ modelling setup including the effect on the total O_3 deposition budget. Subsequently we will discuss the resulting effect on the spatial distribution of the mean ~~background~~ surface O_3 mixing ratios. Then, we will present the comparison of all WRF simulations and CAMS data with the hourly surface observations for the three site selections (High Arctic, Remote and Terrestrial). This section is finalized by the simulated and observed time series for the six High Arctic sites.

3.1 Dry deposition budgets and distribution

265 Figure 3a and Fig. 3b show the mean deposition velocities for the ~~DEFAULT NUDGED~~ and COAREG runs, respectively. As expected, in the ~~DEFAULT NUDGED~~ run (Fig. 3a) the mean V_{d,O_3} to oceans are in the order of 0.05 cm s^{-1} . Furthermore, the spatial distribution shows a relatively low heterogeneity and no increase in deposition ~~velocities~~ towards the warmer waters.

~~In the~~ ~~The~~ COAREG run (Fig. 3b) ~~we find provides a~~ mean V_{d,O_3} in the order of 0.01 cm s^{-1} for the ~~colder waters~~ Arctic ocean $> 70^\circ\text{N}$ up to 0.018 cm s^{-1} for ~~the warmer waters~~. ~~There also appears to be an enhancement of oceans with high~~ 270 ~~I_{aq} concentrations (Fig. C1). Simulated oceanic~~ O_3 deposition ~~to is elevated in~~ coastal waters (e.g. Baltic Sea and around the Bering Strait) with I_{aq} concentrations reaching up to 130 nM compared to ~~30 30-50~~ nM for the open Arctic ocean waters (~~not shown here~~ Fig. C1). This highlights the sensitivity of the COAREG scheme to chemical enhancement with dissolved iodide.

Figure 3c shows the temporal variability in V_{d,O_3} for one of the grid boxes, which is in terms of temporal variability representative for the whole domain. The temporal variability in the ~~DEFAULT run is NUDGED run is mainly~~ governed by temporal 275 variability in r_a . During episodes with high wind speeds ($> 10 \text{ m s}^{-1}$), r_a becomes so small that it is negligible over the constant surface uptake resistance of 2000 s m^{-1} , corresponding to a maximum V_{d,O_3} of 0.05 cm s^{-1} . During episodes with low wind speeds ($< 5 \text{ m s}^{-1}$), reduced turbulent transport poses some additional restriction on O_3 removal with increasing r_a which ~~can reduce~~ ~~reduces~~ the V_{d,O_3} ~~up to ~8%~~ 0.04 cm s^{-1} . In the COAREG run, ~~the~~ temporal variability in O_3 -deposition V_{d,O_3} is also governed by wind speeds that controls the waterside turbulent transport of O_3 in seawater besides atmospheric turbulent 280 transport. For high wind speeds, the waterside turbulent transport increases (Fig. B1) and more O_3 is transported through the turbulent layers. For our simulation, we found that the temporal variability in O_3 deposition due to waterside turbulent transport can be up to $\pm 20\%$ around the mean. Overall, the V_{d,O_3} to oceans in the COAREG run is reduced by $\sim 60\text{-}80\%$ compared to the ~~DEFAULT NUDGED~~ run. The mean V_{d,O_3} to snow and ice is reduced by $\sim 30\text{-}66\%$, from $\sim 0.03 \text{ cm s}^{-1}$ in the ~~DEFAULT NUDGED~~ run to $\sim 0.01 \text{ cm s}^{-1}$ in the COAREG run.

285 The temporal evolution in oceanic O_3 deposition velocities simulated by the COAREG run appears to be on the low side of observed and elsewhere simulated V_{d,O_3} (e.g. Chang et al., 2004; Oh et al., 2008; Ganzeveld et al., 2009). Chang et al. (2004) showed that V_{d,O_3} can increase by a factor of 5 with wind speed increasing from 0 to 20 m s^{-1} . Luhar et al. (2017) (Figure 7) shows a wide range of observed and simulated sensitivities to wind speed. Observations from the TexAQS06 summer campaign in the Gulf of Mexico show a large sensitivity to 10-meter wind speeds even though the model seems unable to 290 capture these high deposition velocities at high wind speeds (Luhar et al., 2017). However, Luhar et al. (2017) also shows

that for the GasEx08 campaign in the cold Southern Ocean the sensitivity of observed and simulated V_{d,O_3} to 10-meter wind speeds is very limited. This limited sensitivity is most accurately represented by the newer two-layer reactivity scheme compared to the older one-layer scheme due to a more limited interaction between chemical reactivity and waterside turbulent transport (Luhar et al., 2017). Furthermore, the variability around the mean presented in Tab. 1 ($0.012 \pm 0.002 \text{ cm s}^{-1}$) seems to correspond to Oh et al. (2008) ($0.016 \pm 0.0015 \text{ cm s}^{-1}$) 1 month simulation including O_3 removal by Γ_{aq} . In this study we show the intramonthly variability in oceanic O_3 deposition which is expected to be relatively low compared to the seasonal variability which will also be driven by temporal changes in solubility and reactivity due to the seasonal changes in SST and Γ_{aq} .

By estimating the total deposition flux for the water, snow/ice and land surfaces we can quantify the total simulated O_3 deposition budget (Tab. 1) for the Arctic modelling domain. Land, not covered with snow or ice, is with 48% the dominant surface type for this specific domain setup in summer. Combined with a relatively high simulated V_{d,O_3} of $\sim 0.45 \text{ cm s}^{-1}$ this is the most important sink, in terms of deposition, of simulated O_3 with ~ 136 – $135 \text{ Tg O}_3 \text{ yr}^{-1}$. The simulated O_3 deposition budget to water bodies, covering 37% of the total surface area, ~~is in the DEFAULT contributes in the NUDGED run~~ $\sim 10\%$ (~ 15.5 – $15.4 \text{ Tg O}_3 \text{ yr}^{-1}$) ~~of to~~ the total O_3 deposition sink. In the COAREG run, this reduces to only $\sim 3\%$ ($\sim 4.6 \text{ Tg O}_3 \text{ yr}^{-1}$) of the total O_3 deposition sink. Simulated O_3 deposition to snow and ice, covering 15% of the total surface area, is the least important deposition sink ~~with removing~~ 4.1 and $\sim 1.7 \text{ Tg O}_3 \text{ yr}^{-1}$ ~~for in~~ the DEFAULT and COAREG runs respectively.

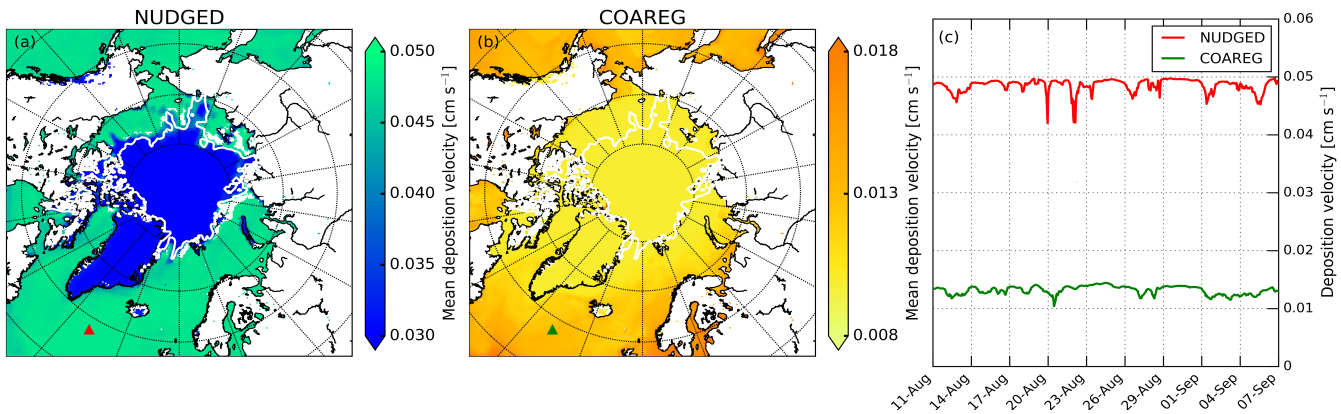


Figure 3. Spatial distribution of the mean simulated O_3 deposition velocity to snow/ice and oceans [cm s^{-1}] for the (a) ~~DEFAULT~~ NUDGED and (b) COAREG simulations and (c) temporal variation in O_3 deposition velocity [cm s^{-1}] for the ~~DEFAULT~~ NUDGED (red) and COAREG (green) simulations. The red and green markers in (a) and (b) indicate the location of the time series shown in (c). To give an indication of the sea ice extent, the white contours show the sea ice fraction of 0.5 at the start of the simulation.

3.2 Simulated and observed monthly mean surface ozone

~~The reduction in O_3 deposition to water and snow/ice surfaces, comparing the DEFAULT and COAREG simulation results (Sect. 3.1, Tab. 1), appears to be limited in terms of relative changes in V_{d,O_3} and the total simulated O_3 deposition budget.~~

Table 1. Mean simulated O_3 deposition velocity (\pm Standard deviation) [$cm\ s^{-1}$] and total simulated deposition budget [$Tg\ O_3\ yr^{-1}$] for the ~~DEFAULT NUDGED~~ and COAREG runs to water, snow/ice and land each representing 37%, 15% and 48% of the total surface area respectively. The standard deviation gives an indication of the spatiotemporal variability in simulated O_3 deposition velocities.

		Water (37%)	Snow/Ice (15%)	Land (48%)	Total (100%)
NUDGED	Deposition velocity (\pm Std.) [$cm\ s^{-1}$]	0.048 <u>0.047</u> (\pm 0.003)	0.030 (\pm 0.000)	0.449 (\pm 0.231 <u>0.225</u>)	
	Deposition budget [$Tg\ O_3\ yr^{-1}$]	15.5 <u>15.4</u>	4.1	132.9 <u>133.4</u>	152.5 <u>152.9</u>
COAREG	Deposition velocity (\pm Std.) [$cm\ s^{-1}$]	0.012 (\pm 0.002)	0.010 (\pm 0.000)	0.448 (\pm 0.251)	
	Deposition budget [$Tg\ O_3\ yr^{-1}$]	4.6	1.7	135.8	142.1

310 Especially contrasting this with the previously mentioned up to \sim 2 orders of magnitude larger V_{d,O_3} to vegetation. However, these relatively small changes do significantly affect the spatial and temporal variation of simulated surface O_3 mixing ratios. Figure 4 shows the spatial distribution in the simulated mean surface O_3 mixing ratios overlain with the observed mean surface O_3 mixing ratios. In the ~~DEFAULT NUDGED~~ and COAREG runs (Fig. 4a and Fig. 4b respectively) we find similar background surface O_3 mixing ratios of \sim 15-20 ppb over the Russian and Canadian/Alaskan land masses. Over Scandinavia, slightly higher 315 background surface O_3 mixing ratios of \sim 20-25 ppb are simulated due to more anthropogenic emissions of precursors in the EDGAR emission inventory and advection of O_3 and its precursors from outside the domain. We As expected, we find a limited effect of reduced deposition to water and snow/ice to the simulated mean O_3 mixing ratios over land. In general, the model appears to be able to simulate the mean observed surface O_3 mixing ratios for the Remote and Terrestrial sites (all sites $< 70^\circ N$) 320 generally well without clear positive or negative bias. However, we Due to the altitude effect higher surface O_3 concentrations are simulated over Greenland even though the deposition velocity to snow and the surrounding oceans is of similar magnitude ($\sim 0.01\ cm\ s^{-1}$).

The reduced O_3 deposition to water and snow/ice surfaces, comparing the NUDGED and COAREG simulation results (Sect. 3.1, Tab. 1), appears to be limited in terms of relative changes in V_{d,O_3} and the total simulated O_3 deposition budget. However, these relatively small changes do substantially affect the simulated spatial distribution of surface O_3 mixing ratios over oceans 325 and sea ice as indicated in Fig. 4. We find that the ~~DEFAULT NUDGED~~ run (Fig. 4a) systematically underestimates the mean observed surface O_3 mixing ratios for the High Arctic sites (all sites $> 70^\circ N$) by \sim 5-10 ppb likely which appears to be caused by an overestimated deposition to ocean, snow and ice surfaces, also further substantiated by the following analysis of short-term variability in O_3 concentrations (Sect. 3.3). Over the Arctic sea ice and oceans the ABL is typically very shallow and atmospheric turbulence is relatively weak. This suppresses vertical mixing and entrainment of O_3 rich air from the free 330 troposphere. Dry deposition of O_3 to the ocean or snow/ice surfaces appears to be an important removal mechanism that has a large impact on O_3 concentrations in these shallow ABLs (Clifton et al., 2020a) both in terms of magnitude but also temporal variability as we will show in Sect. 3.4. In the COAREG run, the background surface O_3 mixing ratios over oceans and Arctic sea ice have increased up to 50%. Furthermore, the reduced deposition to snow/ice has also clearly affected simulated surface O_3 mixing ratios over Greenland. Most importantly, the negative bias in simulated surface O_3 mixing ratios is reduced in the 335 COAREG run with respect to the ~~DEFAULT run~~. This is further examined in NUDGED run (see Sect. 3.3). The CAMS

reanalysis data appears to simulate higher (up to 10 ppb) surface O_3 mixing ratios over land than the two WRF runs. Over sea ice, the magnitude of simulated surface O_3 mixing ratios in CAMS is in between the DEFAULT and COAREG runs. Over Greenland, CAMS simulates mixing ratios of ~ 40 ppb, with a sharp gradient towards the coast. This gradient is less pronounced in the WRF simulations. Both CAMS and WRF appear to underestimate the mean observed (~ 45 ppb) surface O_3 mixing ratios at Summit. The frequency distributions (Fig. 4d) also show that relatively high (25–45 ppb) simulated surface O_3 mixing ratios are more frequent in COAREG and CAMS compared to the DEFAULT and NUDGED runs.

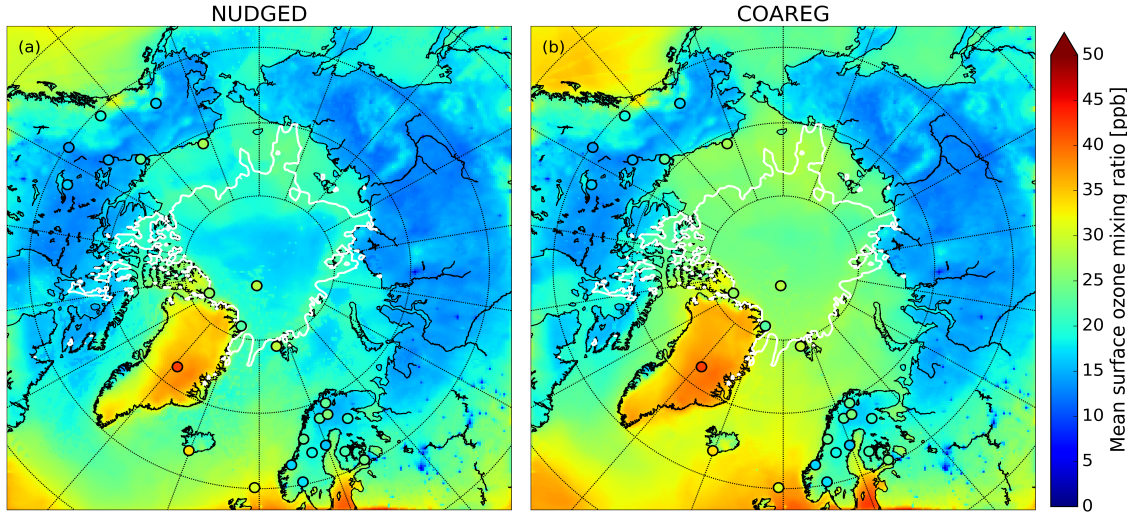


Figure 4. Spatial distribution of the simulated mean surface O_3 mixing ratio [ppb] for the (a) DEFAULT NUDGED and (b) COAREG runs and (c) CAMS data and (d) frequency distributions of surface O_3 mixing ratios ppb over the entire simulation and domain for the DEFAULT (red), NUDGED (yellow), COAREG (green) runs and CAMS data (blue). The filled circles indicate the mean observed ozone mixing ratios [ppb] for the simulated period. To indicate the sea ice extent, the white contours show the sea ice fraction of 0.5 at the start of the simulation.

3.3 Simulated and observed hourly surface ozone

In this section we show how both nudging and the application of the revised deposition scheme can especially improve short-term variability in improves the model prediction scores of surface O_3 concentrations reflected in a comparison of the 345 simulated and observed hourly surface O_3 mixing ratios at the three site selections (High Arctic, Remote and Terrestrial). This is according to our knowledge the first time such a an oceanic O_3 deposition scheme coupled to a meteorology-chemistry model is evaluated against a large dataset of hourly surface O_3 observations. Figure 5 shows a comparison between observed and simulated hourly surface O_3 mixing ratios subdivided in the three site selections: High Arctic, Remote and Terrestrial. For As expected, for the High Arctic sites (Fig. 5, top row) we again find that the DEFAULT run is underestimating the observed 350 surface O_3 mixing ratios with a mean bias of -7.7 ppb. This is consistent to findings in Fig. 4, where the DEFAULT run appears

to underestimate surface O₃ mixing ratios in the High Arctic region. Interestingly, nudging to ERA5 wind, temperature and humidity appears to already reduce some of the bias in the High Arctic by better representing the temporal variability in surface O₃. This is further examined in Sect. 3.4. However, the NUDGED run appears to still underestimate High Arctic surface O₃ with a bias of -3.8 ppb ~~which is also consistent with the findings in Fig. 4, where the NUDGED run appears to underestimate surface O₃ mixing ratios in the High Arctic region.~~ The COAREG run, having a reduced O₃ deposition sink to oceans and snow/ice appears to better represent the ~~background~~ surface O₃ ~~observations~~ with a slight positive bias of 0.3 ppb. The MAE in the COAREG run is reduced to 4.7 ppb from 8.5 and 6.4 for the DEFAULT and NUDGED runs respectively. Furthermore, we find that the CAMS reanalysis data also underestimates surface O₃ in the High Arctic with a bias of -5.0 ppb and a MAE of 6.8 ppb. ~~It has to be noted~~ Note that the performance for all WRF runs and CAMS reanalysis product is varying for each observational site which is further examined in Sect. 3.4.

For the Remote sites (Fig. 5, middle row), having no clear diurnal cycle in surface O₃, we find again an improvement by nudging the WRF model to ERA5 and also by including the mechanistic ocean deposition routine and reduced snow/ice deposition. This improvement appears to be most pronounced for coastal sites like Storhofdi (63.4°N,20.3°W) and Inuvik (68.4°N,133.7°W) ~~having with~~ a reduction in the MAE of 57% and 36% respectively (not shown here). Overall, the improvement for the NUDGED and COAREG runs compared to the DEFAULT run in the Remote site selection is not as significant compared to the High Arctic sites, ~~probably also~~ because of the larger role of O₃ deposition to land and vegetation, which remained unchanged in this study. We find that the CAMS data shows the best performance for the Remote sites with no bias and with a MAE of 5.6 ppb.

For the Terrestrial sites (Fig. 5, bottom row), having a clear diurnal cycle in surface O₃, all WRF runs slightly overestimate the observed surface O₃ mixing ratios with a mean bias up to 1.0 ppb. By nudging WRF to ERA5 the bias is reduced from 7.0 ppb to 6.0 ppb. Reducing the O₃ deposition to oceans and snow/ice increases the bias, but the MAE remains unchanged. The CAMS reanalysis data appears to perform worst for the Terrestrial sites with a bias of 6.4 ppb and a MAE of 8.0 ppb. This might be explained by the lower spatial and temporal resolution ~~in the dataset of CAMS specifically~~ at these sites ~~with having~~ a relatively strong diurnal cycle in ABL dynamics ~~and O₃ concentrations. Interestingly, of all the combinations, we find the largest MAE (8.5 ppb) for the High Arctic sites in the DEFAULT run (Fig. 6a) while we find the lowest MAE (4.7 ppb) for the High Arctic sites in the COAREG run (Fig. 6e). This indicates the high sensitivity of the adjusted ocean, snow and ice surfaces deposition representation to the magnitude and temporal variability in surface O₃ at high latitudes. Because these sites are located far away from the domain boundaries we expect that these model results are to a lesser extent influenced by the boundary conditions compared to the Terrestrial and Remote sites and therefore more sensitive to the O₃ deposition scheme in WRF to vegetation and O₃ concentrations. Also a misrepresentation of emissions of precursor emissions and concentrations and the O₃ deposition to vegetation (Michou et al., 2005; Val Martin et al., 2014) might explain some of the differences.~~

3.4 ~~Temporal~~ Short-term temporal variability of surface ozone in the High Arctic

In Sect. 3.3 we have shown how nudging the WRF model to ERA5 synoptic conditions and revising the O₃ deposition scheme to oceans and snow/ice can improve the model's capability to represent the observed hourly surface O₃ mixing ratios, especially

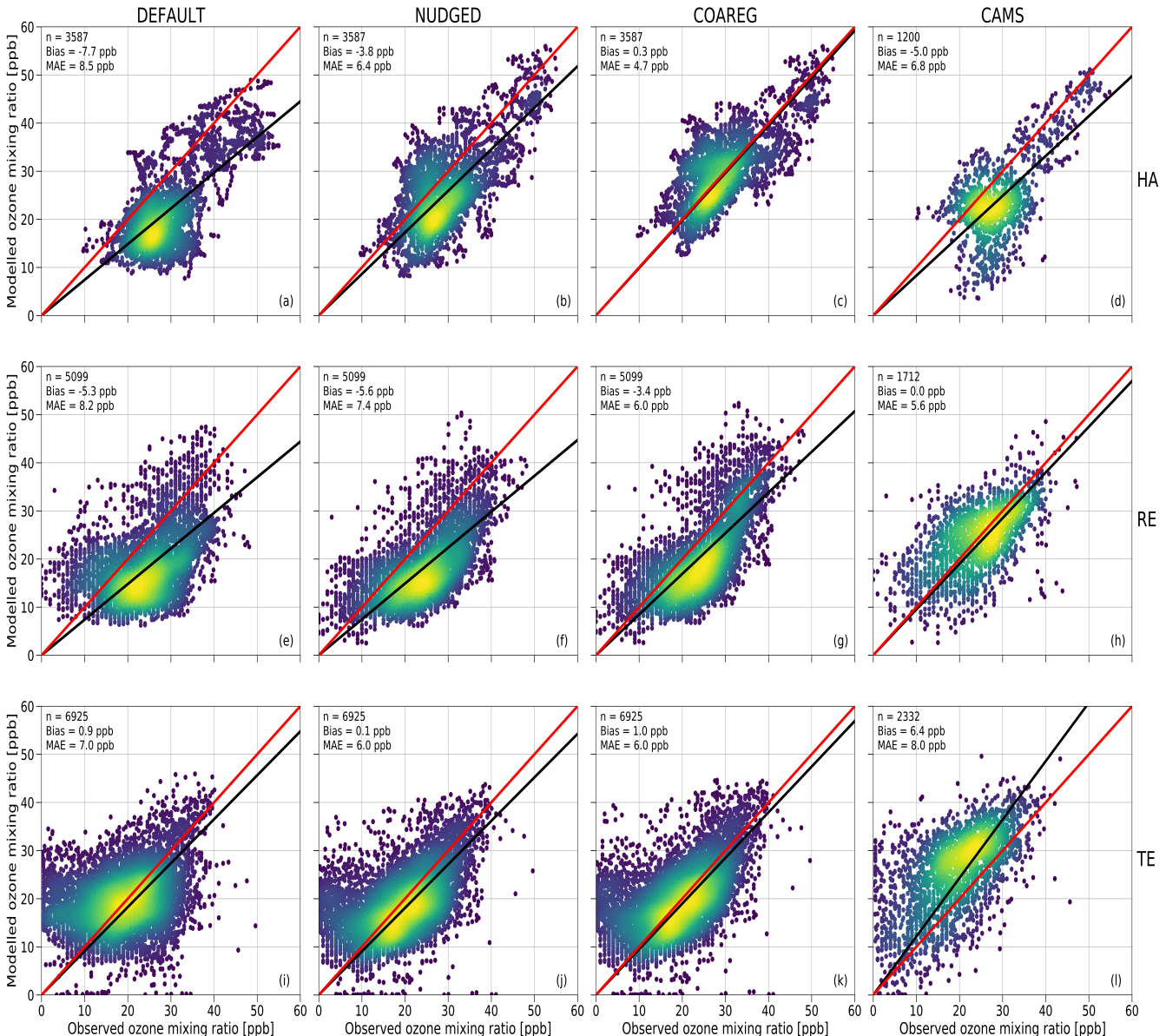


Figure 5. Comparison of the hourly observed and simulated ozone mixing ratios [ppb] for the DEFAULT (a,e,i), NUDGED (b,f,j), COAREG (c,g,k) runs and CAMS data (d,h,l) for the High Arctic (HA) (a-d), Remote (RE) (e-h) and Terrestrial (TE) (i-l) sites. The red line indicates the 1:1 line and the black line indicates the Ordinary Least Squares regression line through the origin. The number of data points (n), Bias [ppb] and Mean Absolute Error (MAE) [ppb] are shown in the top left corner. The colors represent the multivariate kernel density estimation with yellow colors having a higher density.

385 for the High Arctic sites. In this section we show how the ~~three~~ WRF NUDGED and COAREG runs and CAMS represent the temporal variation in High Arctic surface O₃ observations, focusing on a ~~selection~~ 6 out of the 25 measurement sites. ~~These 6 High Arctic sites have been selected due to their deposition footprint being dominated by transport over, and deposition to, ocean and sea-ice covered surfaces.~~ Figure 6 shows the observed and simulated surface O₃ time series for ~~the 6 High Arctic (>70°N) sites~~: ASCOS, Summit, Villum, Zeppelin, Barrow and Alert. Furthermore, Tab. 2 shows the model skill indicators for the High Arctic sites. ~~These skill indicators include the Mean Absolute Error (MAE) that represents the systematic error, the Standard Deviation of Observation minus model Prediction σ_{0-p} that represents the random error and the Pearson-R correlation coefficient (R) that represents the degree of correlation.~~

390 The observations at ASCOS (Fig. 6a) show a sudden increase of surface O₃ mixing ratios from 20 to over 30 ppb around the 17th of August due to advection of relatively ozone rich air during a synoptically active period (Tjernstrom et al., 2012).
395 Only the COAREG run appears to be able to simulate a similar increase in surface O₃ while NUDGED and CAMS show a minor increase ~~and the DEFAULT run shows no increase~~ in simulated surface O₃ ~~at all~~. From the 17th of August onwards, the observations show mixing ratios between 25 and 35 ppb. The WRF simulations indicate advection of air over ocean and ice surfaces during this time period (not shown here). In the COAREG simulation, with less deposition to these surfaces, surface O₃ mixing ratios are less depleted. Only the COAREG run is able to represent these observed mixing ratios with a bias of -2.0
400 ppb whereas the ~~other models simulate NUDGED and CAMS are clearly biased towards~~ lower mixing ratios.

405 At Summit (Fig. 6b), we find a large temporal variability in observed surface O₃ between 30 and 55 ppb. From the 11th of August onwards we find a decreasing trend in observed surface O₃ down to 30 ppb before increasing to 40 ppb around the 17th of August. ~~We find that the DEFAULT run is unable to~~ ~~All models~~ capture this specific event ~~whereas the NUDGED and COAREG runs already appear to capture this event much better~~ in terms of temporal variability even though ~~the model is~~ NUDGED and COAREG are still biased at the observed minimum of 30 ppb. Furthermore, we find that the CAMS reanalysis data represents this specific period very well, also in terms of magnitude. ~~At Summit, the increase of surface O₃ in the COAREG run relative to the NUDGED run mostly reflects the reduction of deposition to snow and ice due to the prevailing katabatic wind flow (Gorter et al., 2014).~~ During episodes with low wind speeds the ABL becomes very stable and shallow during which deposition to snow and ice becomes an important process in removing O₃ in the ABL. In the period between the 14th and 26th
410 of August this reduction in deposition can increase the surface O₃ mixing ratios up to 10 ppb (e.g. 23th of August). In contrast, during episodes with higher wind speeds and deeper ABLs the reduced O₃ deposition to snow hardly affects the simulated surface O₃ concentrations. Interestingly, we find that the NUDGED and COAREG simulations show a larger negative bias (~5-10 ppb) during the period with low wind speeds and shallow ABLs. Over the entire simulated period, CAMS performs best at Summit with a MAE of 3.9 ppb followed by COAREG with a MAE of 6.1 ppb. ~~Interestingly,~~

415 Villum (Fig. 6c) is the only site for which the ~~DEFAULT run performs best in terms of bias and MAE. This run slightly underestimates the observed mixing ratios with a bias of -2.4 ppb.~~ The NUDGED and COAREG runs as well as the CAMS reanalysis data all ~~systematically~~ overestimate the observed mixing ratios, especially later into the simulation. ~~The observations show an increase in O₃ mixing ratios from 10 to 20 ppb in the first three days of the simulation where after it remains between 20 and 30 ppb with relatively low temporal variability compared to some of the other sites (e.g. Summit, Barrow).~~ Both the

420 NUDGED and COAREG runs simulate mixing ratios up to 40 ppb and CAMS simulates maximum surface O₃ mixing ratios of 35 ppb. In terms of representing the magnitude of surface O₃ mixing ratios CAMS performs best with a MAE of 4.5. Zeppelin (Fig. 6d) and Barrow (Fig. 6e) show similar behaviour in terms of observation-model comparison. For both locations, ~~both the DEFAULT run as well as the the~~ CAMS reanalysis data systematically ~~underestimate~~ ~~underestimates~~ observed ozone mixing ratios with ~~biases larger than a~~ ~~biases >~~ 10 ppb. In the NUDGED run, ~~some of the temporal variability is already better represented by WRF and reduces the bias to the bias equals~~ -6.9 and -4.6 ppb for Zeppelin and Barrow, respectively. In the COAREG run the bias is reduced to -1.0 and -0.2 ppb for Zeppelin and Barrow respectively. ~~From the This reduction in bias is, together with ASCOS, the largest among the 6 High Arctic sites and shows the large sensitivity to the representation of O₃ deposition. At Barrow, the dominant wind directions during the simulation period are NW-NE giving a footprint mostly from the Arctic sea ice and ocean. Especially in the period from the 23th of August until the end of the simulation, we find a good example of the importance of a realistic representation of synoptic conditions by nudging and the role of ocean and snow/ice deposition. In this period, the DEFAULT run and CAMS reanalysis data systematically underestimate the 1th of August onward the COAREG run is very accurate in representing the magnitude as well as the temporal variability in observed surface O₃ mixing ratios. Moreover, the COAREG run is representing the observed . During this period, the NUDGED run simulates surface O₃ mixing ratios very well, both in terms of magnitude as well as temporal variability up to 5 ppb lower due to the overestimated deposition to oceans and sea ice. At both sites, the model performance of COAREG is in the same order of magnitude with an MAE, σ_{o-p} and R of ~ 3.5 ppb, 4.2 ppb and 0.65 respectively.~~

425 At Alert (Fig. 6f), ~~the DEFAULT run again underestimates the~~ we find a relatively steady increase in observed surface O₃ mixing ratios even though the bias of -6.4 ppb is not as large as for from 20 ppb at the start of the simulation to 30 ppb at the end of the simulation. The temporal variability, both in observed and simulated surface O₃ appears to be lower compared to

430 some of the other ~~sites~~ High Arctic sites. Again, the statistical parameters such as MAE, σ_{o-p} and R improve in the COAREG run with respect to the NUDGED run. ~~This bias, as well as the MAE, is again decreased for the NUDGED and COAREG runs.~~ At Alert, we find that CAMS has the lowest MAE and σ_{o-p} of 3.0 ppb, ~~but has a slight negative bias of -1.9 ppb and 3.4 ppb respectively.~~

435 The model performance in terms of temporal variability in surface O₃ observations is diagnosed by using the Pearson-R correlation coefficient. ~~Nudging the WRF model to ERA5 meteorological data already improved the representation of the temporal variability especially for sites like Barrow and Summit where the synoptic conditions were likely not represented well. This causes an offset in timing of the advection of different air masses but here also vertical mixing and entrainment of O₃ rich air could play a role.~~ The model performance ~~also~~ improved for all six sites in the COAREG run with respect to the NUDGED run. The COAREG run includes temporal variability in O₃ deposition due to variability in waterside turbulent transport which

440 can explain additional improvements in representing the temporal variability of surface O₃. The COAREG simulation performs best for 5 out of the 6 observational sites in terms of Pearson-R correlation coefficient and is only outperformed by CAMS at Summit. Overall, we find that ~~nudging reduces the bias and MAE for all High Arctic sites except Summit and Villum by better representing the synoptic conditions and therefore the temporal variability in observed surface O₃. Coupling the coupling the~~ WRF model to the mechanistic COAREG ocean-atmosphere exchange representation ~~further decreases the bias and MAE~~

455 ~~decreases the MAE and σ_{O_3} for all High Arctic sites except for Villum by better representing the magnitude of, but also temporal variability in observed surface O_3 . The CAMS reanalysis data is performing well for some locations (e.g. Summit, Alert) while for Zeppelin and Barrow the discrepancy is among the largest we found in the observation-model comparison.~~

Table 2. ~~Bias~~ MAE [ppb], ~~MAE~~ σ_{O_3} [ppb] and Pearson-R correlation coefficient (R) [-] for the ~~DEFAULT~~, NUDGED ~~and~~ COAREG runs and CAMS reanalysis data at the ASCOS, Summit, Villum, Zeppelin, Barrow and Alert observational sites. The lowest model error and highest correlation have been made bold for every site.

	ASCOS			Summit															
	Bias	MAE	σ_{O_3}	R	Bias	MAE	σ_{O_3}												
DEFAULT	-11.5	11.5	0.24	-5.3	7.4	0.17	-2.4	4.5	0.5	-9.5	9.5	0.61	-12.4	12.4	-0.18	-6.4	6.6	0.43	NUDGED
COAREG							-9.4	9.4	4.3						-5.5	7.5	7.0		
CAMS							-2.0	3.1	3.2	0.67					-4.0	6.1	5.8		
							-6.8	7.5	4.5	0.07					-2.6	3.9	4.3		

4 Discussion

460 ~~In this study, we demonstrate the role~~ This study demonstrates the impact of a mechanistic representation of ocean-atmosphere O_3 exchange to simulate the magnitude and temporal variability of hourly surface O_3 concentrations in the Arctic region. We show that the ~~model~~ modelled sensitivity of the surface O_3 concentrations to the representation of O_3 to ocean, ice and snow surfaces is high, even though the total deposition budget is an order of magnitude smaller than the deposition to land and vegetation. Using a mechanistic ~~representation of oceanic~~ O_3 deposition ~~to oceans and reducing the representation and reduced~~ O_3 deposition to snow and ice greatly reduced the negative bias in surface O_3 , especially in the high Arctic. Furthermore, the 465 short-term temporal variability in surface O_3 was also better represented by the mechanistic representation of oceanic O_3 deposition by also accounting for temporal variations in the driving processes of ~~oceanic~~ O_3 deposition such as waterside turbulent transport.

470 Our main objective was to address the ~~role~~ impact of a mechanistic oceanic O_3 deposition representation, including spatial and temporal variability, on the magnitude and temporal variability of surface O_3 concentrations ~~and to evaluate this with~~ ~~a large dataset of 25 observational sites in and around the Arctic~~. We show that Arctic surface O_3 concentrations are ~~very~~ sensitive to the representation of O_3 deposition ~~. We did not address include in the presented analysis how the nudging and representation of Arctic O_3 deposition further affects the contribution to the Arctic O_3 budget e.g. by changes in photochemistry and stratosphere-troposphere exchange and advection. For such a budget analysis it would be best to perform at least one year of simulation to also address the seasonal cycles in deposition, photochemistry and long range transport which is computationally~~ ~~too expensive in WRF. Regarding oceanic to oceans and sea-ice especially at coastal sites and sites with latitudes $>70^\circ\text{N}$. At sites with a more terrestrial footprint (e.g. Norway, Sweden, Finland), the comparison of modelled and observed surface O_3 concentrations also shows a discrepancy. As expected, this discrepancy has not been resolved introducing the more mechanistic representation of O_3 deposition oceans and modified snow/sea-ice deposition rate. In terms of deposition, these sites are mostly~~



Figure 6. Temporal evolution of hourly surface O₃ mixing ratios [ppb] for the **DEFAULT** (red), NUDGED (yellow) and COAREG (green) runs, CAMS data (blue crosses) and observations (black dots) at ASCOS ($\sim 87.4^\circ\text{N}, \sim 6.0^\circ\text{W}$), Summit ($72.6^\circ\text{N}, 38.5^\circ\text{W}$), Villum ($81.6^\circ\text{N}, 16.7^\circ\text{W}$), Zeppelin ($78.9^\circ\text{N}, 11.0^\circ\text{E}$), Barrow ($71.3^\circ\text{N}, 156.6^\circ\text{W}$) and Alert ($82.5^\circ\text{N}, 62.3^\circ\text{W}$).

influenced by O₃ deposition to vegetation and land (e.g. Silva and Heald, 2018; Wong et al., 2019; Clifton et al., 2020b). In the
480 WRF simulations, dry deposition of O₃ to vegetation (mostly land-use class: 'wooded tundra') amounts to \sim 0.2-1.0 cm s⁻¹ with a clear diurnal cycle. Dry deposition of O₃ to 'bare tundra' is in the order of 0.1-0.15 cm s⁻¹ which is slightly higher than observed by Van Dam et al. (2015). A detailed analysis of O₃ deposition ~~this would also include long-term changes in sea ice cover and oceanic biogeochemistry. The major constraint in this model setup is the lack of oceanic to land and vegetation is beyond the scope of this study and would require a different strategy, e.g. direct comparison with O₃ flux measurements (e.g. Van Dam et al., 2016).~~ However, a better understanding and model representation of the drivers of O₃ deposition ~~measurements over the Arctic ocean. The COAREG exchange routine has been built and validated using to vegetation and land, including the diurnal and seasonal variability of these drivers (Lin et al., 2019), is anticipated to also result in a better representation of short-term variability of surface O₃ over land.~~

The COAREG scheme has been developed and validated against eddy-covariance measurements over mostly (sub-)tropical
490 waters (Bariteau et al., 2010; Helmig et al., 2012). The COAREG routine has been ~~further developed and used applied~~ to study the effects of wind speed and sea state on ocean atmosphere gas transfer (Blomquist et al., 2017; Bell et al., 2017; Porter et al., 2020). We do expect that these main drivers, being waterside turbulent transfer and chemical enhancement with dissolved iodide, ~~held for oceans also controls oceanic O₃ deposition~~ at high latitudes. ~~Using indirect information to evaluate Indirect evaluation of oceanic O₃ deposition through comparison of surface O₃ observations instead of direct oceanic O₃ flux measurements we show that the addition of indicates that including~~ this mechanistic representation of O₃ deposition ~~results in a better representation of both the improves both the modelled~~ magnitude and temporal variability in surface O₃ observations. However, ~~the exact magnitude and variability in Arctic a lack of oceanic O₃ deposition could not be evaluated using flux measurements flux~~ hampers the direct model evaluation of the high-latitude O₃ deposition flux. This is expected to be soon resolved by getting access to O₃ flux observations collected in the Multidisciplinary drifting Observatory
495 for the Study of Arctic Climate (MOSAiC) 1-year field campaign.

Furthermore, we have reduced the deposition to snow and ice ~~based on a study by Helmig et al. (2007a). The results of that study also further following Helmig et al. (2007a) and (Clifton et al., 2020b). Results of Helmig et al. (2007a) also~~ motivated
500 follow-up observational and modelling studies aiming at the development of ~~, similar to COAREG for oceanic O₃ deposition,~~ more mechanistic representations of O₃ deposition to snow/ice covered surfaces. For example, efforts have been made to simulate O₃ dynamics in and above the snowpack using a 1D model setup to ~~evaluate explain~~ observations of O₃ and NO_x concentrations measured above and inside the Summit snowpack (Van Dam et al., 2015). This 1D modelling study showed the main role of aqueous-phase oxidation of O₃ with formic acid in the snowpack (Murray et al., 2015). Comparable 1D modelling studies focused on assessing the role of catalytic ozone loss via bromine radical chemistry in the snowpack interstitial air (Thomas et al., 2011; Toyota et al., 2014). However, these studies mainly ~~arrived at conclusions regarding addressed~~ the role
510 of some of this snowpack chemistry in explaining, partly observed, O₃ concentrations and not so much on snow-atmosphere O₃ fluxes and derived deposition rates that would corroborate the inferred very small O₃ deposition rates by Helmig et al. (2007a). Clifton et al. (2020b) summarized that accurate process-based modelling of O₃ deposition to snow requires better understanding of the underlying processes and dependencies. An eddy-covariance system has been set up as part of the MO-

SAIC campaign and will provide year-round O₃ deposition fluxes to several land surface types such as open ocean and sea ice with fluctuating snow cover. These measurements will further enhance our understanding of O₃ deposition in shallow ABLs at high latitudes (Clifton et al., 2020a) and the further role in regional atmospheric chemistry.

In this study we used the COAREG transfer algorithm version 3.6 which is extended with a two-layer scheme for surface resistance compared to the previous versions (Fairall et al., 2007, 2011) and similar to the work by Luhar et al. (2018). Oceanic iodide (I_{aq}) is generally deemed to be the most significant reactant for O₃ in oceanic water (Chang et al., 2004). Similar to Pound et al. (2019) we have used the global I_{aq} distribution by Sherwen et al. (2019) on a spatial resolution of 0.125° × 0.125°. This distribution replaces the previously applied iodide estimations only using SST (Chance et al., 2014; MacDonald et al., 2014). Using the Sherwen et al. (2019) distribution for August/September we found relatively high I_{aq} concentrations ranging from 30 to 130 nM whereas the MacDonald et al. (2014) estimation would imply I_{aq} concentrations ranging from 5 to 50 nM. This implies that in the WRF setup, using the Sherwen et al. (2019) I_{aq} distribution, the cold Arctic ocean is still quite effective in removing O₃ from the surface waters having I_{aq} as a reactant. On the global scale, the most recent I_{aq} climatology by Sherwen et al. (2019) most accurately represents the observed I_{aq} compared to estimations only using SST (Chance et al., 2014; MacDonald et al., 2014). However, Sherwen et al. (2019) noted that the I_{aq} estimations at high latitudes (north of ≥ 65°N) are very poorly constrained by the observational datasets and are therefore also an uncertainty in this study on Arctic O₃. Therefore, new I_{aq} measurements at high latitudes, for example those performed during the MOSAiC expedition, will be very useful to better constrain the global I_{aq} distributions as well as mechanistic oceanic O₃ deposition representations. The WRF simulations in this study did not consider Luhar et al. (2018). Our WRF simulations excluded the additional role of chlorophyll, Dissolved Organic Matter (DOM) or other species such as DMS on chemical enhancement of O₃ in surface waters. Experimental studies have shown that DMS, chlorophyll, or other reactive organics, can may enhance the removal of O₃ at the sea surface (Chang et al., 2004; Clifford et al., 2008; Chang et al., 2004; Clifford et al., 2008; Reeser et al., 2009; Martino et al., 2012). The global modelling study by Ganzeveld et al. (2009) included a chlorophyll-O₃ reactivity that increased linearly with chlorophyll concentration as a proxy for the role of DOM in oceanic O₃ deposition. The addition of this reaction significantly Including this reaction substantially enhances O₃ deposition to coastal waters such that actually observed O₃ deposition to these coastal waters is well reproduced (Ganzeveld et al., 2009). Other studies on oceanic O₃ deposition such as Luhar et al. (2017); Pound et al. (2019) did not consider ignored the potential role of DOM-O₃ chemistry in oceanic O₃ deposition. The study by Luhar et al. (2018), which did not explicitly consider coastal waters, even suggested that including such a reaction deteriorates the comparison with O₃ flux observations above open oceans. A considerable uncertainty in the DOM-O₃ reaction is the second-order rate coefficient but also the magnitude and variability in oceanic DOM concentrations (Luhar et al., 2018). To test the sensitivity of our model setup to other reactants in the surface water we have performed an additional sensitivity analysis including the chlorophyll-O₃ and DMS-O₃ reactions from Ganzeveld et al. (2009). Regarding chlorophyll we have used the monthly Oceanic chlorophyll concentrations have been retrieved from the 9 × 9 km resolution MODIS chlorophyll- α concentrations dataset available at https://modis.gsfc.nasa.gov/data/dataproducts/chlor_a.php (last access: 14 Aug 2020). For DMS Chlorophyll- α concentrations are typically < 3 mg m⁻³ for open oceans up to 25 mg m⁻³ for coastal waters. For oceanic DMS concentrations, we use the monthly climatology from Lana et al. (2011). The sensitivity study with chlorophyll as extra reactant indicated a slight increase (up

to 5%) in deposition to coastal waters with chlorophyll concentrations up to 25 mg m^{-3} . However, the resulting effect on 550 surface O_3 concentrations was not significant due to the large fraction of oceans with very low ($< 3 \text{ mg m}^{-3}$) chlorophyll- α concentrations. Also the reactions with oceanic DMS appear to be weak due to relatively low DMS concentrations in August/September. A These sensitivity studies indicate that I_{aq} is the main driver of chemical reactivity of O_3 in the Arctic ocean in summer. However a potential sensitivity of these reactants on Arctic O_3 deposition could especially be expected in the 555 spring to summer transition following from algal blooms (Stefels et al., 2007; Riedel et al., 2008). However, in springtime the removal of Arctic O_3 near the surface is also largely affected by halogen chemistry (Pratt et al., 2013; Thomas et al., 2013). In this season, the (Pratt et al., 2013; Thomas et al., 2013; Yang et al., 2020) and which is known to explain observed surface O_3 mixing ratios can drop dropping to 0 ppb (Halfacre et al., 2014). If this study we have limited our analysis to a period in which However, this feature is of less relevance for the presented study with the evaluation being focused on August/September and 560 when the role of halogen chemistry is not important deemed being less important (Yang et al., 2020).
565 We nudged the WRF model to the ECMWF ERA5 reanalysis product to ensure a fair model evaluation with observations due to a better representation of the synoptic conditions. This indicated the important role of the model representation of meteorologmeteorology, e.g. advection of polluted air and mixing/entrainment of O_3 in the ABL, in representing the observed surface O_3 concentrations. An improvement in simulated synoptic conditions was also found when initializing and nudging the model with ECMWF ERA-Interim data (Dee et al., 2011). This indicates that both reanalysis products have a better representation of the actual synoptic conditions than the free running WRF model. The model evaluation was set up at a resolution of $30 \times 30 \text{ km}$ which is in the order of the ERA5 reanalysis data ($0.25^\circ \times 0.25^\circ$) used for initial conditions, boundary conditions and nudging. Nudging, but then to the NCEP FNL reanalysis data, was also applied in a study by Marelle et al. (2017) using WRF for quasi-hemispheric simulations of aerosols and O_3 in the Arctic at a resolution of $100 \times 100 \text{ km}$. In this study Here, we opted for a $30 \times 30 \text{ km}$ setup km grid spacing because we expect that the main drivers of tropospheric 570 O_3 (chemical production and destruction, stratosphere-troposphere transport, dry deposition and mixing/advection processes) can be sufficiently resolved at this resolution grid spacing especially over the relatively homogeneous ocean, ice and snow surfaces. However, we do realize that the use of a $30 \times 30 \text{ km}$ might have caused some issues in such a coarse grid spacing may have hampered representing local air flow phenomena such as katabatic winds (Klein et al., 2001) which could explain some of the mismatch at sites like Villum (Nguyen et al., 2016). Another justification for the $30 \times 30 \text{ km}$ resolution km grid spacing 575 was to limit computational time and to have a large enough domain to cover the entire region above 60°N to conduct a large pan-Arctic evaluation while at the same time having all observational sites far enough from the domain boundaries to limit the effect of the imposed meteorological and chemical boundary conditions.
580 We plan to use a similar model setup, but then at a higher resolution or using a 1D-setup, to evaluate the O_3 In general, the relatively scarce Arctic observations introduces constraints to modelling studies and limits the potential of these results to be extrapolated to other seasons and lower latitudes. In this case, this includes the uncertainty in the magnitude and distribution of driving factors of oceanic O_3 concentration and flux measurements in and around the Arctic sea ice deposition such as I_{aq} (Sherwen et al., 2019) or DOM. New I_{aq} measurements at high latitudes, for example those performed during the year-round MOSAiC expedition. These observations will likely give insight in the role, will be very useful to better constrain the global

585 ~~I_{aq} distributions as well as mechanistic oceanic O₃ deposition representations. Measurements of O₃ deposition to sea ice and concentrations and deposition fluxes to the Arctic ocean during different seasons (e.g. wintertime with no photo-chemistry or springtime with active halogen chemistry) and for a wide range of meteorological conditions. Furthermore, this local flux and concentration evaluation can be extended to species such as DMS which is now also included in the COAREG version that is coupled to WRF. However, this lacks a combined seawater and atmospheric concentration and flux dataset to conduct a local validation or a similar pan-Arctic distributed surface network such as presented here for O₃ to perform an indirect regional assessment.~~ can assist to better constrain these modelling setups in terms of magnitude and temporal variability and potentially indicate of the sensitivity to other environmental factors such as wind speed in waters with low reactivity. Furthermore, including the role of halogen chemistry (Pratt et al., 2013; Thompson et al., 2017) might give an indication of the combined role of halogens and oceanic deposition in removing O₃ and explaining the magnitude and short- but also long-term variability of O₃ concentrations in the High Arctic.

595 **5 Conclusions**

600 The mesoscale meteorology-chemistry model Polar-WRF-Chem was coupled to the Coupled Ocean-Atmosphere Response Experiment Gas transfer algorithm (COAREG) to allow for a mechanistic representation of ocean-atmosphere exchange of ~~trace gases. Regarding the deposition of ozone (O₃) to ocean waters, this mechanistic representation includes the O₃. This scheme represents~~ effects of molecular diffusion, solubility, waterside turbulent transfer and chemical enhancement of O₃ uptake through its reactions with dissolved iodide. The ~~new mechanistic representation~~ GOAREG scheme replaces the constant surface uptake resistance approach often applied in ACTMs. Furthermore, we have increased the ~~modelled~~ O₃ surface uptake resistance to snow and ice. In total, three simulations were performed: 1) default WRF setup (DEFAULT), 2) nudged to ERA5 synoptic conditions (NUDGED) and 3) with adjustments to O₃ surface uptake resistance as described above (COAREG). Furthermore, the CAMS global reanalysis data product has also been included in the ~~comparison to illustrate some limitations in the Arctic presented evaluation on High Arctic surface O₃.~~ This CAMS product is widely used in air quality assessments and to constrain regional scale modelling experiments. ~~This provides additional information on the quality of the CAMS data products but also on potential issues in the representation of O₃ sources and sinks, e.g., oceanic and snow/sea-ice deposition, for the High Arctic.~~ The modelling approach was set up for ~~an one month at the~~ end-of-summer period in 2008 and evaluated against hourly surface O₃ at 25 sites for latitudes > 60°N including observations over the Arctic sea ice as part of the ASCOS campaign.

610 Using the mechanistic representation of ocean-atmosphere exchange, O₃ deposition velocities were simulated in the order of 0.01 cm s⁻¹ compared to ~0.05 cm s⁻¹ in the constant surface uptake resistance approach. In the COAREG run, the spatial variability (0.01 to 0.018 cm s⁻¹) in the mean O₃ deposition velocities expressed the sensitivity to chemical enhancement with dissolved iodide. The temporal variability of O₃ deposition velocities (up to ±20% around the mean) is governed by surface wind speeds and expressed differences in waterside turbulent transport. In the constant surface uptake resistance approach, there is no spatial variability in O₃ deposition velocities and the temporal variability is determined by the aerodynamic resis-

tance term that can be significant at low wind speeds. Using the mechanistic representation of ocean-atmosphere exchange reduced the total simulated O₃ deposition budget to water bodies by ~~~70%~~^{a factor of 3.3 compared to the default constant ocean uptake rate approach} and the increase in surface uptake resistance to snow and ice reduced the deposition budget by ~~~60%~~^{a factor of 2.4.}

Despite the fact that O₃ deposition to oceans, snow and ice surfaces only constitutes a small term in the total O₃ deposition budget (~~more than~~> 90% of the deposition is to land), we find a substantial sensitivity to the simulated surface O₃ mixing ratios. In the COAREG run, the simulated mean monthly surface O₃ mixing ratios have increased up to 50% in the typically shallow Arctic ABL above the oceans and ~~(sea-)ice~~ sea-ice relative to the ~~DEFAULT~~ ~~NUDGED~~ run. The mechanistic representation of O₃ deposition to oceans, but also nudging to ERA5 synoptic conditions, resulted in a substantial improved representation of surface O₃ observations, especially for the High Arctic sites having latitudes > 70 °N. The DEFAULT run ~~was underestimating~~ ~~underestimated~~ the observed surface O₃ mixing ratios with a bias of -7.7 ppb whereas the NUDGED and COAREG runs had a bias of -3.8 ppb and 0.3 ppb, respectively. The evaluation of the WRF runs at individual High Arctic sites showed that using the mechanistic representation of O₃ deposition to oceans and nudging the model to ERA5 better represents the surface O₃ observations in terms of magnitude as well as short-term temporal variability. ~~The evaluation of the CAMS reanalysis product also indicated limitations to represent the observed surface O₃ at the High Arctic in terms of magnitude and temporal variability. Similar to DEFAULT and NUDGED~~ ~~Similar to the NUDGED run~~, CAMS underestimated High Arctic observed surface O₃ with a bias of -5.0 ppb indicating that for this product the deposition removal mechanism to oceans and snow/ice might also be overestimated ~~and should be reconsidered~~.

This study highlights the ~~role impact~~ of a mechanistic representation of oceanic O₃ deposition on Arctic surface O₃ concentrations at a high (hourly) temporal resolution. It ~~mostly~~ corroborates the findings of global scale studies (~~e.g.~~ Ganzeveld et al., 2009; Luhar et al., 2013) and recommends that the representation of O₃ deposition to oceans and snow/ice in global and regional scale ACTMs should be revised. This revision is needed not only to better quantify the O₃ budget at the global scale, but also to better represent the observed magnitude and short-term temporal variability of surface O₃ at the regional scale. ~~In addition, explicit consideration of the mechanisms involved in O₃ removal by the oceans (and sea-ice/snow pack) are essential to also evaluate the role of potentially important feedback mechanisms and future trends in- and the role of O₃ in Arctic climate change as a function of declining sea ice cover, increasing emissions and changes in oceanic biogeochemical conditions.~~ On the regional scale, this study also has implications ~~on the fate of the Arctic O₃ budget~~ ~~for methods to quantify future trends in Arctic tropospheric O₃, Arctic air pollution and climate in a period of declining sea ice and increasing local emissions of precursors. Furthermore, this study also serves as a preparatory study for an extensive evaluation of the upcoming year-round Arctic O₃, and other climate active trace gases, concentration and deposition flux measurements as part of the MOSAiC campaign.~~

Code availability. The COAREG algorithm is available at ftp://ftp1.esrl.noaa.gov/BLO/Air-Sea/bulkalg/cor3_6/gasflux36/, last access: 10 September 2020. The coupled Polar-WRF-Chem model, model output and post-processing scripts are available upon request.

Author contributions. JGMB, LNG and GJS designed the experiment. JGMB performed the Polar-WRF-Chem simulations and performed
650 the analysis. JGMB, LNG, GJS and MCK wrote the manuscript.

Competing interests. The authors declare that they have no conflict of interest.

Acknowledgements. J.G.M. Barten is financially supported by the Dutch Research Council (NWO) as part of the Netherlands Polar Programme (NPP) under the project name "Multi-scale model analysis of Arctic surface-boundary layer exchange of climate-active trace gases and aerosol precursors" with grant no. 866.18.004. The authors acknowledge the Polar-WRF-Chem developers and support as well as the
655 COAREG developers and in special Chris Fairall. [Furthermore, the authors thank the three anonymous reviewers for their extensive reviews as well as Owen Cooper and Ashok Luhar for providing short comments on the manuscript.](#)

Appendix A: WRF physical and chemical parameterization schemes.

Table A1. WRF physical and chemical parameterization schemes.

WRF option	Configuration
Physical parameterizations	
Microphysics	WSM5 (Hong et al., 2004)
Long wave radiation	RRTMG (Iacono et al., 2008)
Short wave radiation	RRTMG (Iacono et al., 2008)
Surface layer	Monin-Obukhov (Janjić, 2001)
Land surface	Noah (Chen and Dudhia, 2001)
Boundary layer	MYJ (Janjić, 1994)
Cumulus	Kain-Fritsch (Kain, 2004)
Chemistry	
Gas-phase	CBM-Z (Gery et al., 1989; Zaveri and Peters, 1999)
Photolysis	Fast-J (Wild et al., 2000)
Emissions	
Anthropogenic	EDGAR (Janssens-Maenhout et al., 2017)
Biogenic	MEGAN (Guenther et al., 2012)
Boundary conditions	
<u>Meteorology</u>	<u>ERA5 ($0.25^\circ \times 0.25^\circ$) (Hersbach et al., 2020)</u>
<u>Chemistry</u>	<u>CAMS ($0.75^\circ \times 0.75^\circ$) (Inness et al., 2019)</u>

Appendix B: Formulation of the air- and waterside resistance terms

The exchange velocity, in this case deposition, of ozone (V_{d,O_3}) [m s^{-1}] is calculated from the waterside resistance (r_w) [s m^{-1}] and air side resistance terms ($r_a + r_b$) [s m^{-1}] as follows:

$$V_{d,O_3} = \frac{1}{\alpha r_w + r_a + r_b}. \quad (\text{B1})$$

Here, α [-] is the dimensionless solubility of O_3 in sea water calculated from SST [K] following Morris (1988) as

$$\alpha = 10^{-0.25 - 0.013(SST - 273.16)} \quad (\text{B2})$$

and the waterside resistance term (r_w) is calculated as

$$r_w = \sqrt{a * D} \frac{\Psi K_1(\xi_\delta) \cosh \lambda + K_0(\xi_\delta) \sinh \lambda}{\Psi K_1(\xi_\delta) \sinh \lambda + K_0(\xi_\delta) \cosh \lambda}. \quad (\text{B3})$$

Here, a [s^{-1}] is the chemical reactivity of O_3 with I_{aq} calculated with the second order rate coefficient [$\text{M}^{-1} \text{s}^{-1}$] from Magi et al. (1997) and the I_{aq} concentrations [M] from Sherwen et al. (2019):

$$a = k \cdot [\text{I}_{\text{aq}}^-] = \exp\left(\frac{-8772.2}{SST} + 51.5\right) \cdot [\text{I}_{\text{aq}}^-]. \quad (\text{B4})$$

In Eq. B3, D [$\text{m}^2 \text{s}^{-1}$] is the molecular diffusivity of O_3 in ocean water and is calculated from the kinematic viscosity ν [$\text{m}^2 \text{s}^{-1}$] and the waterside Schmidt number (S_{cw}) [-] as

$$D = \frac{\nu}{S_{cw}} = \frac{\mu}{\rho} / [\sqrt{44/48} \cdot \exp(-0.055 \cdot SST + 22.63)] \quad (\text{B5})$$

where μ [$\text{kg m}^{-1} \text{s}^{-1}$] is the dynamic viscosity of seawater and ρ [kg m^{-3}] is the density of seawater.

Finally, the air side resistance terms ($r_a + r_b$) [s m^{-1}] of the deposition velocity in Eq. B1 are calculated as

$$r_a + r_b = [C_d^{-1/2} + 13.3 S_c^{1/2} - 5 + \frac{\log(S_c)}{2\kappa}] / u_{*,a} \quad (\text{B6})$$

where C_d [-] is the momentum drag coefficient, S_c [-] is the Schmidt number for ozone in the atmosphere, κ is the Von Karman constant (0.4) and $u_{*,a}$ [m s^{-1}] is the friction velocity in the atmosphere. The $r_a + r_b$ term is typically in the order of 100 s m^{-1} (Fairall et al., 2011).

Compared to COAREG version 3.1 (Fairall et al., 2007, 2011), COAREGv3.6 is extended with a two-layer scheme based on Luhar et al. (2018). This extension is included in the second term of the waterside resistance term (Eq. B3). Here, $\Psi = \sqrt{1 + (\kappa u_{*,w} \delta_m / D)}$

$\xi_\delta = \sqrt{2 a b (\delta_m + b D / 2)}$, and $\lambda = \delta_m \sqrt{a / D}$ with $b = 2 / (\kappa u_{*,w})$. This part of the equation is a function of the chemical reactivity a [s^{-1}] (Eq. B4), the waterside friction velocity $u_{*,w}$ [m s^{-1}], the molecular diffusivity of O_3 in ocean water (Eq. B5) and δ_m [m] representing the depth of the interface between the top water layer and the underlying turbulent layer. In this study we have applied $\delta_m = c_0 \sqrt{D/a}$ with $c_0 = 0.4$ based on Luhar et al. (2018). $K_0(\xi_\delta)$ and $K_1(\xi_\delta)$ are the modified Bessel

functions of the second kind of order 0 and 1, respectively. For more information on the derivation of the formulas please visit

685 Fairall et al. (2007, 2011); Luhar et al. (2018).

Figure B1 shows the sensitivity of the COAREG routine coupled to WRF to the environmental factors wind speed, SST and Iodide concentration. The sensitivity to wind speeds (Fig. B1a) expresses the role of waterside turbulent transport and aerodynamic resistance. For low wind speeds waterside turbulent transport is limited and therefore limits the exchange of O_3 from the atmosphere to the ocean. At high wind speeds, the dry deposition of O_3 is limited by chemical reactivity of O_3 with I_{aq} at typical Arctic SSTs of 5 °C and I_{aq} concentrations of 60 nM (see also Fig. C1). At very low wind speeds ($< 3 \text{ m s}^{-1}$) the aerodynamic resistance poses an extra restriction on the ocean-atmosphere exchange of O_3 . The sensitivity to SST (Fig. B1b) mostly represents the role of solubility (Eq. B2) with warmer waters having a lower solubility. In contrast to Luhar et al. (2018), the SST is not used to calculate the I_{aq} concentrations and does therefore not show a positive correlation. The sensitivity to I_{aq} (Fig. B1c) represents the role of chemical enhancement which is stronger than the generally compensating effect of solubility in warmer waters for typical Arctic conditions.

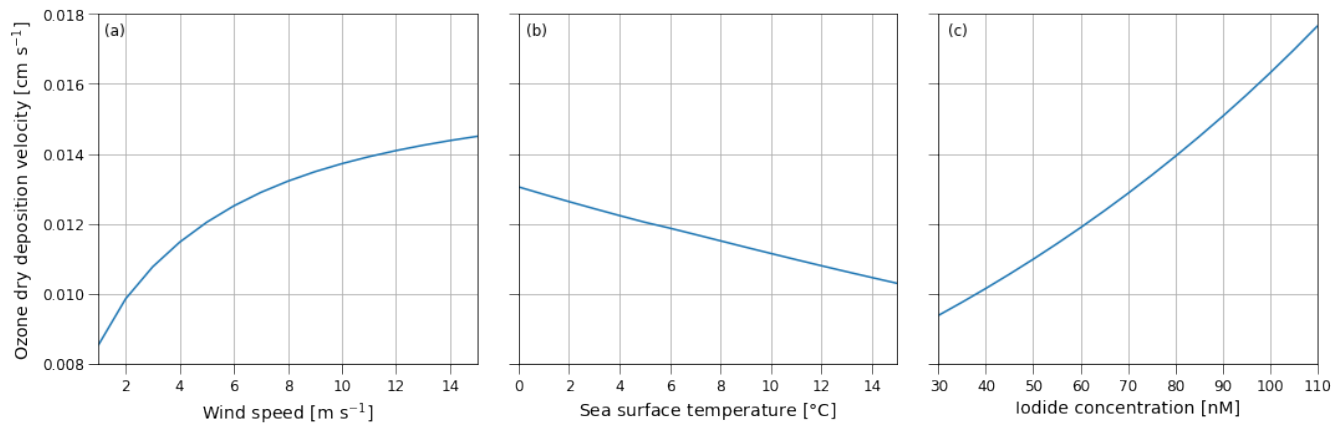


Figure B1. Sensitivity of the ozone dry deposition velocity from COAREG to the environmental factors 10-meter wind speed [m s⁻¹] (a), sea surface temperature [°C] (b) and sea surface Iodide concentration [nM] (c) using typical values of 10-meter wind speed, sea surface temperature and Iodide concentration of 5 m s⁻¹, 5 °C and 60 nM respectively. Note that the sensitivity to sea surface temperature does not include effects of increasing reactivity but mostly represents the effect of reduced solubility (Eq. B2).

695

Appendix C: Spatial distribution of oceanic Iodide

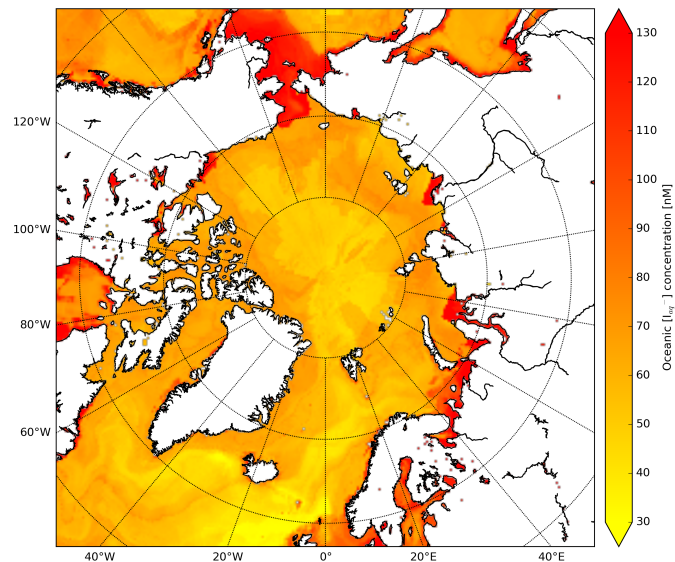


Figure C1. Spatial distribution of Sherwen et al. (2019) oceanic Iodide concentrations [nM] at the start of the simulation.

Appendix D: Surface ozone measurement sites.

Table D1. Surface ozone measurement sites subdivided in the 'High Arctic', 'Remote' and 'Terrestrial' site selections.

Name	Abbreviation	Group	Latitude [°N]	Longitude [°E]
Alert	ALT	High Arctic	82.5	-62.3
ASCOS	ASC	High Arctic	~ 87.4	~ -6.0
Barrow	BRW	High Arctic	71.3	-156.6
Zeppelin	NYA	High Arctic	78.9	11.9
Summit	SUM	High Arctic	72.6	-38.5
Villum	VIL	High Arctic	81.6	-16.7
Denali NP	DEN	Remote	63.7	-149.0
Esrang	ESR	Remote	67.9	21.1
Karasjok	KAS	Remote	69.5	25.2
Inuvik	INU	Remote	68.4	-133.7
Lerwick	SIS	Remote	60.1	-1.2
Pallas	PAL	Remote	68.0	21.1
Storhofdi	ICE	Remote	63.4	-20.3
Yellowknife	YEL	Remote	62.5	-114.4
Ahtari	AHT	Terrestrial	62.6	24.2
Bredkalen	BRE	Terrestrial	63.9	15.3
Fort Liard	FOR	Terrestrial	60.2	-123.5
Hurdal	HUR	Terrestrial	60.4	11.1
Karvatn	KRV	Terrestrial	62.8	8.9
Norman Wells	NOR	Terrestrial	65.3	-123.8
Oulanka	OUX	Terrestrial	66.3	29.4
Tustervatn	TUV	Terrestrial	65.8	13.9
Vindeln	VDI	Terrestrial	64.3	19.8
Virolahti	VIR	Terrestrial	60.5	27.7
Whitehorse	WHI	Terrestrial	60.7	-135.0

References

Ainsworth, E. A., Yendrek, C. R., Sitch, S., Collins, W. J., and Emberson, L. D.: The effects of tropospheric ozone on net primary productivity
700 and implications for climate change, *Annual review of plant biology*, 63, 637–661, 2012.

Arnold, S. R., Law, K. S., Brock, C. A., Thomas, J. L., Starkweather, S. M., von Salzen, K., Stohl, A., Sharma, S., Lund, M. T., Flanner,
M. G., et al.: Arctic air pollution: Challenges and opportunities for the next decade, *Elementa: Science of the Anthropocene*, 2016.

Bariteau, L., Helmig, D., Fairall, C., Hare, J., Hueber, J., and Lang, E.: Determination of oceanic ozone deposition by ship-borne eddy
covariance flux measurements, *Atmospheric Measurement Techniques*, 3, 441–455, 2010.

705 Bell, T. G., Landwehr, S., Miller, S. D., De Bruyn, W. J., Callaghan, A. H., Scanlon, B., Ward, B., Yang, M., and Saltzman, E. S.: Estimation of
bubble-mediated air-sea gas exchange from concurrent DMS and CO₂ transfer velocities at intermediate-high wind speeds, *Atmospheric
Chemistry and Physics*, 17, 9019–9033, 2017.

Blomquist, B., Brumer, S., Fairall, C., Huebert, B., Zappa, C., Brooks, I., Yang, M., Bariteau, L., Prytherch, J., Hare, J., et al.: Wind speed and
sea state dependencies of air-sea gas transfer: Results from the high wind speed gas exchange study (HiWinGS), *Journal of Geophysical
710 Research: Oceans*, 122, 8034–8062, 2017.

Bromwich, D. H., Otieno, F. O., Hines, K. M., Manning, K. W., and Shilo, E.: Comprehensive evaluation of polar weather research and
forecasting model performance in the Antarctic, *Journal of Geophysical Research: Atmospheres*, 118, 274–292, 2013.

Chance, R., Baker, A. R., Carpenter, L., and Jickells, T. D.: The distribution of iodide at the sea surface, *Environmental Science: Processes
& Impacts*, 16, 1841–1859, 2014.

715 Chang, W., Heikes, B. G., and Lee, M.: Ozone deposition to the sea surface: chemical enhancement and wind speed dependence, *Atmospheric
Environment*, 38, 1053–1059, 2004.

Chen, F. and Dudhia, J.: Coupling an advanced land surface–hydrology model with the Penn State–NCAR MM5 modeling system. Part I:
Model implementation and sensitivity, *Monthly weather review*, 129, 569–585, 2001.

Chen, X., Quéléver, L. L., Fung, P. L., Kesti, J., Rissanen, M. P., Bäck, J., Keronen, P., Junninen, H., Petäjä, T., Kerminen, V.-M., et al.:
720 Observations of ozone depletion events in a Finnish boreal forest, *Atmospheric Chemistry and Physics*, 18, 49–63, 2018.

Clifford, D., Donaldson, D., Brigante, M., D’Anna, B., and George, C.: Reactive uptake of ozone by chlorophyll at aqueous surfaces,
Environmental science & technology, 42, 1138–1143, 2008.

Clifton, O., Paulot, F., Fiore, A., Horowitz, L., Correa, G., Baublitz, C., Fares, S., Goded, I., Goldstein, A., Gruening, C., et al.: Influence of
dynamic ozone dry deposition on ozone pollution, *Journal of Geophysical Research: Atmospheres*, 125, e2020JD032398, 2020a.

725 Clifton, O. E., Fiore, A. M., Massman, W. J., Baublitz, C. B., Coyle, M., Emberson, L., Fares, S., Farmer, D. K., Gentine, P., Gerosa, G.,
et al.: Dry deposition of ozone over land: processes, measurement, and modeling, *Reviews of Geophysics*, 58, e2019RG000670, 2020b.

Cooper, O. R., Parrish, D., Ziemke, J., Cupeiro, M., Galbally, I., Gilge, S., Horowitz, L., Jensen, N., Lamarque, J.-F., Naik, V., et al.: Global
distribution and trends of tropospheric ozone: An observation-based review, 2014.

Cooper, O. R., Schultz, M. G., Schröder, S., Chang, K.-L., Gaudel, A., Benítez, G. C., Cuevas, E., Fröhlich, M., Galbally, I. E., Molloy, S.,
730 et al.: Multi-decadal surface ozone trends at globally distributed remote locations, *Elementa: Science of the Anthropocene*, 8, 2020.

Dee, D. P., Uppala, S. M., Simmons, A., Berrisford, P., Poli, P., Kobayashi, S., Andrae, U., Balmaseda, M., Balsamo, G., Bauer, d. P., et al.:
The ERA-Interim reanalysis: Configuration and performance of the data assimilation system, *Quarterly Journal of the royal meteorological
society*, 137, 553–597, 2011.

Fairall, C., Helmig, D., Ganzeveld, L., and Hare, J.: Water-side turbulence enhancement of ozone deposition to the ocean, *Atmospheric Chemistry and Physics*, 2007, 443–451, 2007.

Fairall, C., Yang, M., Bariteau, L., Edson, J., Helmig, D., McGillis, W., Pezoa, S., Hare, J., Huebert, B., and Blomquist, B.: Implementation of the Coupled Ocean-Atmosphere Response Experiment flux algorithm with CO₂, dimethyl sulfide, and O₃, *Journal of Geophysical Research: Oceans*, 116, 2011.

Fairall, C. W., Bradley, E. F., Rogers, D. P., Edson, J. B., and Young, G. S.: Bulk parameterization of air-sea fluxes for tropical ocean-global atmosphere coupled-ocean atmosphere response experiment, *Journal of Geophysical Research: Oceans*, 101, 3747–3764, 1996.

Fan, S.-M., Wofsy, S. C., Bakwin, P. S., Jacob, D. J., and Fitzjarrald, D. R.: Atmosphere-biosphere exchange of CO₂ and O₃ in the central Amazon forest, *Journal of Geophysical Research: Atmospheres*, 95, 16 851–16 864, 1990.

Gallagher, M., Beswick, K., and Coe, H.: Ozone deposition to coastal waters, *Quarterly Journal of the Royal Meteorological Society*, 127, 539–558, 2001.

Ganzeveld, L., Helmig, D., Fairall, C., Hare, J., and Pozzer, A.: Atmosphere-ocean ozone exchange: A global modeling study of biogeochemical, atmospheric, and waterside turbulence dependencies, *Global Biogeochemical Cycles*, 23, 2009.

Gaudel, A., Cooper, O. R., Chang, K.-L., Bourgeois, I., Ziemke, J. R., Strode, S. A., Oman, L. D., Sellitto, P., Nédélec, P., Blot, R., et al.: Aircraft observations since the 1990s reveal increases of tropospheric ozone at multiple locations across the Northern Hemisphere, *Science Advances*, 6, eaba8272, 2020.

Gery, M. W., Whitten, G. Z., Killus, J. P., and Dodge, M. C.: A photochemical kinetics mechanism for urban and regional scale computer modeling, *Journal of Geophysical Research: Atmospheres*, 94, 12 925–12 956, 1989.

Gorter, W., Van Angelen, J., Lenaerts, J., and Van den Broeke, M.: Present and future near-surface wind climate of Greenland from high resolution regional climate modelling, *Climate dynamics*, 42, 1595–1611, 2014.

Grell, G. A., Peckham, S. E., Schmitz, R., McKeen, S. A., Frost, G., Skamarock, W. C., and Eder, B.: Fully coupled “online” chemistry within the WRF model, *Atmospheric Environment*, 39, 6957–6975, 2005.

Guenther, A., Jiang, X., Heald, C., Sakulyanontvittaya, T., Duhl, T., Emmons, L., and Wang, X.: The Model of Emissions of Gases and Aerosols from Nature version 2.1 (MEGAN2. 1): an extended and updated framework for modeling biogenic emissions, 2012.

Halfacre, J., Knepp, T., Shepson, P., Thompson, C., Pratt, K., Li, B., Peterson, P., Walsh, S., Simpson, W., Matrai, P., et al.: Temporal and spatial characteristics of ozone depletion events from measurements in the Arctic, *Atmospheric Chemistry and Physics*, 14, 4875, 2014.

Hardacre, C., Wild, O., and Emberson, L.: An evaluation of ozone dry deposition in global scale chemistry climate models, *Atmospheric Chemistry and Physics*, 15, 6419–6436, 2015.

Helmig, D., Ganzeveld, L., Butler, T., and Oltmans, S.: The role of ozone atmosphere-snow gas exchange on polar, boundary-layer tropospheric ozone? a review and sensitivity analysis, 2007a.

Helmig, D., Oltmans, S. J., Carlson, D., Lamarque, J.-F., Jones, A., Labuschagne, C., Anlauf, K., and Hayden, K.: A review of surface ozone in the polar regions, *Atmospheric Environment*, 41, 5138–5161, 2007b.

Helmig, D., Cohen, L. D., Bocquet, F., Oltmans, S., Grachev, A., and Neff, W.: Spring and summertime diurnal surface ozone fluxes over the polar snow at Summit, Greenland, *Geophysical research letters*, 36, 2009.

Helmig, D., Lang, E., Bariteau, L., Boylan, P., Fairall, C., Ganzeveld, L., Hare, J., Hueber, J., and Pallandt, M.: Atmosphere-ocean ozone fluxes during the TexAQS 2006, STRATUS 2006, GOMECC 2007, GasEx 2008, and AMMA 2008 cruises, *Journal of Geophysical Research: Atmospheres*, 117, 2012.

Hersbach, H., Bell, B., Berrisford, P., Hirahara, S., Horányi, A., Muñoz-Sabater, J., Nicolas, J., Peubey, C., Radu, R., Schepers, D., et al.: The ERA5 global reanalysis, *Quarterly Journal of the Royal Meteorological Society*, 2020.

Hines, K. M. and Bromwich, D. H.: Development and testing of Polar Weather Research and Forecasting (WRF) model. Part I: Greenland ice sheet meteorology, *Monthly Weather Review*, 136, 1971–1989, 2008.

775 Hong, S.-Y., Dudhia, J., and Chen, S.-H.: A revised approach to ice microphysical processes for the bulk parameterization of clouds and precipitation, *Monthly weather review*, 132, 103–120, 2004.

Iacono, M. J., Delamere, J. S., Mlawer, E. J., Shephard, M. W., Clough, S. A., and Collins, W. D.: Radiative forcing by long-lived greenhouse gases: Calculations with the AER radiative transfer models, *Journal of Geophysical Research: Atmospheres*, 113, 2008.

Inness, A., Ades, M., Agustí-Panareda, A., Barré, J., Benedictow, A., Blechschmidt, A.-M., Dominguez, J. J., Engelen, R., Eskes, H., Flemming, J., Huijnen, V., Jones, L., Kipling, Z., Massart, S., Parrington, M., Peuch, V.-H., Razinger, M., Remy, S., Schulz, M., and Suttie, M.: The CAMS reanalysis of atmospheric composition, *Atmospheric Chemistry and Physics*, 19, 3515–3556, <https://doi.org/10.5194/acp-19-3515-2019>, <https://www.atmos-chem-phys.net/19/3515/2019/>, 2019.

780 Janjić, Z. I.: The step-mountain eta coordinate model: Further developments of the convection, viscous sublayer, and turbulence closure schemes, *Monthly weather review*, 122, 927–945, 1994.

785 Janjić, Z. I.: Nonsingular implementation of the Mellor-Yamada level 2.5 scheme in the NCEP Meso model, 2001.

Janssens-Maenhout, G., Crippa, M., Guizzardi, D., Muntean, M., Schaaf, E., Dentener, F., Bergamaschi, P., Pagliari, V., Olivier, J., Peters, J., et al.: EDGAR v4.3.2 Global Atlas of the three major Greenhouse Gas Emissions for the period 1970–2012, *Earth Syst. Sci. Data Discuss.*, 2017.

Kain, J. S.: The Kain–Fritsch convective parameterization: an update, *Journal of applied meteorology*, 43, 170–181, 2004.

790 Kavassalis, S. C. and Murphy, J. G.: Understanding ozone-meteorology correlations: A role for dry deposition, *Geophysical Research Letters*, 44, 2922–2931, 2017.

Klein, T., Heinemann, G., Bromwich, D. H., Cassano, J. J., and Hines, K. M.: Mesoscale modeling of katabatic winds over Greenland and comparisons with AWS and aircraft data, *Meteorology and Atmospheric Physics*, 78, 115–132, 2001.

795 Lana, A., Bell, T., Simó, R., Vallina, S., Ballabrera-Poy, J., Kettle, A., Dachs, J., Bopp, L., Saltzman, E., Stefels, J., et al.: An updated climatology of surface dimethylsulfide concentrations and emission fluxes in the global ocean, *Global Biogeochemical Cycles*, 25, 2011.

Law, K. S., Roiger, A., Thomas, J. L., Marelle, L., Raut, J.-C., Dalsøren, S., Fuglestvedt, J., Tuccella, P., Weinzierl, B., and Schlager, H.: Local Arctic air pollution: Sources and impacts, *Ambio*, 46, 453–463, 2017.

Lee, D. S., Holland, M. R., and Falla, N.: The potential impact of ozone on materials in the UK, *Atmospheric Environment*, 30, 1053–1065, 1996.

800 Lelieveld, J. and Dentener, F. J.: What controls tropospheric ozone?, *Journal of Geophysical Research: Atmospheres*, 105, 3531–3551, 2000.

Lin, M., Horowitz, L. W., Payton, R., Fiore, A. M., and Tonnesen, G.: US surface ozone trends and extremes from 1980 to 2014: quantifying the roles of rising Asian emissions, domestic controls, wildfires, and climate, *Atmospheric Chemistry and Physics*, 17, 2943–2970, 2017.

Lin, M., Malyshev, S., Shevliakova, E., Paulot, F., Horowitz, L. W., Fares, S., Mikkelsen, T. N., and Zhang, L.: Sensitivity of ozone dry deposition to ecosystem-atmosphere interactions: A critical appraisal of observations and simulations, *Global Biogeochemical Cycles*, 33, 805 1264–1288, 2019.

Lin, M., Horowitz, L. W., Xie, Y., Paulot, F., Malyshev, S., Shevliakova, E., Finco, A., Gerosa, G., Kubistin, D., and Pilegaard, K.: Vegetation feedbacks during drought exacerbate ozone air pollution extremes in Europe, *Nature Climate Change*, 10, 444–451, 2020.

Luhar, A. K., Galbally, I. E., Woodhouse, M. T., and Thatcher, M.: An improved parameterisation of ozone dry deposition to the ocean and its impact in a global climate-chemistry model, *Atmospheric Chemistry and Physics*, 17, 3749, 2017.

810 Luhar, A. K., Woodhouse, M. T., and Galbally, I. E.: A revised global ozone dry deposition estimate based on a new two-layer parameterisation for air-sea exchange and the multi-year MACC composition reanalysis., *Atmospheric Chemistry & Physics*, 18, 2018.

MacDonald, S., Gómez Martín, J., Chance, R., Warriner, S., Saiz-Lopez, A., Carpenter, L., and Plane, J.: A laboratory characterisation of inorganic iodine emissions from the sea surface: dependence on oceanic variables and parameterisation for global modelling, *Atmospheric Chemistry and Physics*, 14, 5841–5852, 2014.

815 Magi, L., Schweitzer, F., Pallares, C., Cherif, S., Mirabel, P., and George, C.: Investigation of the uptake rate of ozone and methyl hydroperoxide by water surfaces, *The Journal of Physical Chemistry A*, 101, 4943–4949, 1997.

Mahmood, R., von Salzen, K., Norman, A.-L., Galfi, M., and Levasseur, M.: Sensitivity of Arctic sulfate aerosol and clouds to changes in future surface seawater dimethylsulfide concentrations., *Atmospheric Chemistry & Physics*, 19, 2019.

Marelle, L., Thomas, J. L., Raut, J.-C., Law, K. S., Jalkanen, J.-P., Johansson, L., Roiger, A., Schlager, H., Kim, J., Reiter, A., et al.: Air 820 quality and radiative impacts of Arctic shipping emissions in the summertime in northern Norway: from the local to the regional scale, 2016.

Marelle, L., Raut, J.-C., Law, K. S., Berg, L. K., Fast, J. D., Easter, R. C., Shrivastava, M., and Thomas, J. L.: Improvements to the WRF-Chem 3.5.1 model for quasi-hemispheric simulations of aerosols and ozone in the Arctic, *Geoscientific Model Development*, 10, 3661–3677, <https://doi.org/10.5194/gmd-10-3661-2017>, <https://gmd.copernicus.org/articles/10/3661/2017/>, 2017.

825 Marelle, L., Raut, J.-C., Law, K. S., and Duclaux, O.: Current and Future Arctic Aerosols and Ozone From Remote Emissions and Emerging Local Sources—Modeled Source Contributions and Radiative Effects, *Journal of Geophysical Research: Atmospheres*, 123, 12–942, 2018.

Martino, M., Lézé, B., Baker, A. R., and Liss, P. S.: Chemical controls on ozone deposition to water, *Geophysical research letters*, 39, 2012.

Michou, M., Laville, P., Serça, D., Fotiadi, A., Bouchou, P., and Peuch, V.-H.: Measured and modeled dry deposition velocities over the ESCOMPTE area, *Atmospheric Research*, 74, 89–116, 2005.

830 Morris, J.: The aqueous solubility of ozone—A review, *Ozone news*, 1, 14–16, 1988.

Muller, J. B., Dorsey, J. R., Flynn, M., Gallagher, M. W., Percival, C. J., Shallcross, D. E., Archibald, A., Roscoe, H. K., Obbard, R. W., Atkinson, H. M., et al.: Energy and ozone fluxes over sea ice, *Atmospheric environment*, 47, 218–225, 2012.

Murray, K. A., Kramer, L. J., Doskey, P. V., Ganzeveld, L., Seok, B., Van Dam, B., and Helmig, D.: Dynamics of ozone and nitrogen oxides at Summit, Greenland. II. Simulating snowpack chemistry during a spring high ozone event with a 1-D process-scale model, *Atmospheric 835 Environment*, 117, 110–123, 2015.

Nguyen, Q. T., Glasius, M., Sørensen, L. L., Jensen, B., Skov, H., Birmili, W., Wiedensohler, A., Kristensson, A., Nøjgaard, J. K., and Massling, A.: Seasonal variation of atmospheric particle number concentrations, new particle formation and atmospheric oxidation capacity at the high Arctic site Villum Research Station, *Station Nord*, 2016.

Nuvolone, D., Petri, D., and Voller, F.: The effects of ozone on human health, *Environmental Science and Pollution Research*, 25, 8074–8088, 840 2018.

Oh, I.-B., Byun, D. W., Kim, H.-C., Kim, S., and Cameron, B.: Modeling the effect of iodide distribution on ozone deposition to seawater surface, *Atmospheric Environment*, 42, 4453–4466, 2008.

Oltmans, S., Lefohn, A., Shadwick, D., Harris, J., Scheel, H., Galbally, I., Tarasick, D., Johnson, B., Brunke, E.-G., Claude, H., et al.: Recent tropospheric ozone changes—A pattern dominated by slow or no growth, *Atmospheric Environment*, 67, 331–351, 2013.

845 Paatero, J., Vaattovaara, P., Vesterius, M., Meinander, O., Makkonen, U., Kivi, R., Hyvärinen, A., Asmi, E., Tjernström, M., and Leck, C.: Finnish contribution to the arctic summer cloud ocean study (ASCOS) expedition, Arctic Ocean 2008, *Geophysica*, 45, 119–146, 2009.

Padro, J.: Summary of ozone dry deposition velocity measurements and model estimates over vineyard, cotton, grass and deciduous forest in summer, *Atmospheric Environment*, 30, 2363–2369, 1996.

Pausata, F., Pozzoli, L., Vignati, E., and Dentener, F.: North Atlantic Oscillation and tropospheric ozone variability in Europe: model analysis and measurements intercomparison., *Atmospheric Chemistry & Physics*, 12, 2012.

850 Pedregosa, F., Varoquaux, G., Gramfort, A., Michel, V., Thirion, B., Grisel, O., Blondel, M., Prettenhofer, P., Weiss, R., Dubourg, V., et al.: Scikit-learn: Machine learning in Python, *the Journal of machine Learning research*, 12, 2825–2830, 2011.

Porter, J., de Bruyn, W., Miller, S., and Saltzman, E.: Air/sea transfer of highly soluble gases over coastal waters, *Geophysical Research Letters*, 47, no–no, 2020.

855 Pound, R. J., Sherwen, T., Helmig, D., Carpenter, L. J., and Evans, M. J.: Influences of oceanic ozone deposition on tropospheric photochemistry, *Atmospheric Chemistry and Physics Discussions*, pp. 1–25, 2019.

Prados Roman, C., Cuevas, C. A., Fernandez, R. P., Kinnison, D. E., Lamarque, J. F., and Saiz-lopez, A.: A negative feedback between anthropogenic ozone pollution and enhanced ocean emissions of iodine, 2015.

Pratt, K. A., Custard, K. D., Shepson, P. B., Douglas, T. A., Pöhler, D., General, S., Zielcke, J., Simpson, W. R., Platt, U., Tanner, D. J., et al.: 860 Photochemical production of molecular bromine in Arctic surface snowpacks, *Nature Geoscience*, 6, 351–356, 2013.

Reeser, D. I., Jammoul, A., Clifford, D., Brigante, M., D'Anna, B., George, C., and Donaldson, D.: Photoenhanced reaction of ozone with chlorophyll at the seawater surface, *The Journal of Physical Chemistry C*, 113, 2071–2077, 2009.

Riedel, A., Michel, C., Gosselin, M., and LeBlanc, B.: Winter–spring dynamics in sea-ice carbon cycling in the coastal Arctic Ocean, *Journal of Marine Systems*, 74, 918–932, 2008.

865 Schmale, J., Arnold, S., Law, K. S., Thorp, T., Anenberg, S., Simpson, W., Mao, J., and Pratt, K.: Local Arctic air pollution: A neglected but serious problem, *Earth's Future*, 6, 1385–1412, 2018.

Sherwen, T., Chance, R. J., Tinel, L., Ellis, D., Evans, M. J., and Carpenter, L. J.: A machine learning based global sea-surface iodide distribution, *Earth System Science Data Discussions*, pp. 1–40, 2019.

Silva, S. J. and Heald, C. L.: Investigating dry deposition of ozone to vegetation, *Journal of Geophysical Research: Atmospheres*, 123, 870 559–573, 2018.

Stefels, J., Steinke, M., Turner, S., Malin, G., and Belviso, S.: Environmental constraints on the production and removal of the climatically active gas dimethylsulphide (DMS) and implications for ecosystem modelling, *Biogeochemistry*, 83, 245–275, 2007.

Tarasick, D., Galbally, I. E., Cooper, O. R., Schultz, M. G., Ancellet, G., Leblanc, T., Wallington, T. J., Ziemke, J., Liu, X., Steinbacher, M., et al.: 875 Tropospheric Ozone Assessment Report: Tropospheric ozone from 1877 to 2016, observed levels, trends and uncertainties, *Elementa: Science of the Anthropocene*, 7, 2019.

Thomas, J. L., Stutz, J., Lefer, B., Huey, L. G., Toyota, K., Dibb, J. E., and von Glasow, R.: Modeling chemistry in and above snow at Summit, Greenland – Part 1: Model description and results, *Atmospheric Chemistry and Physics*, 11, 4899–4914, <https://doi.org/10.5194/acp-11-4899-2011>, <https://acp.copernicus.org/articles/11/4899/2011/>, 2011.

Thomas, J. L., Raut, J.-C., Law, K. S., Marelle, L., Ancellet, G., Ravetta, F., Fast, J. D., Pfister, G., Emmons, L. K., Diskin, G. S., Weinheimer, A., Roiger, A., and Schlager, H.: Pollution transport from North America to Greenland during summer 2008, *Atmospheric Chemistry and Physics*, 13, 3825–3848, <https://doi.org/10.5194/acp-13-3825-2013>, <https://www.atmos-chem-phys.net/13/3825/2013/>, 2013.

Thompson, C. R., Shepson, P. B., Liao, J., Huey, L. G., Cantrell, C., Flocke, F., and Orlando, J.: Bromine atom production and chain propagation during springtime Arctic ozone depletion events in Barrow, Alaska, *Atmospheric Chemistry and Physics*, 17, 3401, 2017.

Tjernstrom, M., Birch, C. E., Brooks, I. M., Shupe, M. D., Persson, P. O. G., Sedlar, J., Mauritsen, T., Leck, C., Paatero, J., Szczodrak, M., et al.: Meteorological conditions in the central Arctic summer during the Arctic Summer Cloud Ocean Study (ASCOS), *Atmospheric Chemistry and Physics*, 12, 6863–6889, 2012.

Toyota, K., McConnell, J., Staebler, R., and Dastoor, A.: Air–snowpack exchange of bromine, ozone and mercury in the springtime Arctic simulated by the 1-D model PHANTAS–Part 1: In-snow bromine activation and its impact on ozone, *Atmos. Chem. Phys.*, 14, 4101–4133, 2014.

Toyota, K., Dastoor, A. P., and Ryzhkov, A.: Parameterization of gaseous dry deposition in atmospheric chemistry models: Sensitivity to aerodynamic resistance formulations under statically stable conditions, *Atmospheric Environment*, 147, 409–422, 2016.

Val Martin, M., Heald, C., and Arnold, S.: Coupling dry deposition to vegetation phenology in the Community Earth System Model: Implications for the simulation of surface O₃, *Geophysical Research Letters*, 41, 2988–2996, 2014.

Van Dam, B., Helmig, D., Toro, C., Doskey, P., Kramer, L., Murray, K., Ganzeveld, L., and Seok, B.: Dynamics of ozone and nitrogen oxides at Summit, Greenland: I. Multi-year observations in the snowpack, *Atmospheric Environment*, 123, 268–284, 2015.

Van Dam, B., Helmig, D., Doskey, P. V., and Oltmans, S. J.: Summertime surface O₃ behavior and deposition to tundra in the Alaskan Arctic, *Journal of Geophysical Research: Atmospheres*, 121, 8055–8066, 2016.

Wentz, F. and Meissner, T.: AMSR-E/Aqua Daily L3 Global Ascending/Descending .25x.25 deg Ocean Grids, Version 2., 2004.

Wesely, M.: Parameterization of surface resistances to gaseous dry deposition in regional-scale numerical models, *Atmospheric Environment* (1967), 23, 1293–1304, 1989.

Wesely, M. and Hicks, B.: A review of the current status of knowledge on dry deposition, *Atmospheric environment*, 34, 2261–2282, 2000.

Wild, O., Zhu, X., and Prather, M. J.: Fast-J: Accurate simulation of in-and below-cloud photolysis in tropospheric chemical models, *Journal of Atmospheric Chemistry*, 37, 245–282, 2000.

Wong, A. Y., Geddes, J. A., Tai, A. P., and Silva, S. J.: Importance of dry deposition parameterization choice in global simulations of surface ozone, *Atmospheric Chemistry and Physics*, 19, 14 365–14 385, 2019.

Yang, X., Blechschmidt, A.-M., Bognar, K., McClure-Begley, A., Morris, S., Petropavlovskikh, I., Richter, A., Skov, H., Strong, K., Tarasick, D. W., et al.: Pan-Arctic surface ozone: modelling vs. measurements, *Atmospheric Chemistry and Physics*, 20, 15 937–15 967, 2020.

Young, P. J., Naik, V., Fiore, A. M., Gaudel, A., Guo, J., Lin, M., Neu, J., Parrish, D., Rieder, H., Schnell, J., et al.: Tropospheric Ozone Assessment Report: Assessment of global-scale model performance for global and regional ozone distributions, variability, and trends, *Elementa: Science of the Anthropocene*, 6, 2018.

Zaveri, R. A. and Peters, L. K.: A new lumped structure photochemical mechanism for large-scale applications, *Journal of Geophysical Research: Atmospheres*, 104, 30 387–30 415, 1999.

Zeller, K.: Wintertime ozone fluxes and profiles above a subalpine spruce–fir forest, *Journal of Applied Meteorology*, 39, 92–101, 2000.

Zhou, P., Ganzeveld, L., Rannik, Ü., Zhou, L., Gierens, R., Taipale, D., Mammarella, I., and Boy, M.: Simulating ozone dry deposition at a boreal forest with a multi-layer canopy deposition model, *Atmospheric Chemistry and Physics*, 17, 1361–1379, 2017.